TURUN YLIOPISTO
UNIVERSITY OF TURKU

ORGANOMERCURY OLIGONUCLEOTIDES AS ARTIFICIAL RIBONUCLEASES

Lange Yakubu Saleh

ORGANOMERCURY OLIGONUCLEOTIDES AS ARTIFICIAL RIBONUCLEASES

Lange Yakubu Saleh

University of Turku

Faculty of Science
Department of Chemistry
Chemistry
Doctoral programme in Exact Science (EXACTUS)

Supervised by

Professor Tuomas Lönnberg
Department of Chemistry
University of Turku
Turku, Finland

Adjunct Professor Mikko Ora
Department of Chemistry
University of Turku
Turku, Finland

Reviewed by

Professor James K. Bashkin
Department of Chemistry and Biochemistry
University of Missouri-St. Louis
St. Louis, Missouri, United States

Professor David R. W. Hodgson
Department of Chemistry
University of Durham
Durham, United Kingdom

Opponent

Professor Roger Strömberg
Department of Laboratory Medicine
Karolinska Institutet
Stockholm, Sweden

To my lovely family & friends

UNIVERSITY OF TURKU
Faculty of Science
Department of Chemistry
Chemistry
LANGE YAKUBU SALEH: Organomercury Oligonucleotides as Artificial
Ribonucleases
Doctoral Dissertation, 88 pp.
Doctoral Programme in Exact Sciences
May 2024

ABSTRACT

Antisense oligonucleotides (ASOs) leverage the natural catalytic activity of RNases H to target specific RNA sequences for degradation. However, the challenge lies in incorporating chemical modifications into ASOs to enhance cellular delivery, stability and binding affinity without compromising their ability to recruit RNases H. This delicate balance often poses limitations in achieving optimal therapeutic outcomes. Artificial ribonucleases (aRNases) are designed to selectively cleave RNA sequences, mirroring the function of natural ribonucleases but tailored for specific applications. These synthetic counterparts effectively cleave phosphodiester bonds in RNA molecules, enabling diverse applications, including targeted degradation of specific RNA sequences within cells.

The current state-of-the-art aRNases that rely on metal ions, such as Cu(II) or Zn(II) in coordination complexes, face challenges in highly diluted and metal-deficient conditions, such as those found in the intracellular medium. aRNases having the catalytic metal ions bonded to carbon resist dissociation even at extreme dilution, thus promising to combine the stability of organic compounds with the catalytic efficacy of metal complexes. We chose Hg(II) as the catalytic metal ion for the hydrolytic stability, and ready availability of arylmercury complexes.

This thesis presents kinetic studies conducted across various pH ranges on the cleavage of RNA model molecule adenylyl-3′,5′-(2′,3′-O-methyleneadenosine) catalyzed by mercury (II) and an arylmercury complex. Both agents facilitated the cleavage of the RNA model compound. Additionally, two oligonucleotide conjugates, featuring the same sequence but differing in the 5′-terminal organomercury moiety, were synthesized using established methods. One was synthesized through direct mercuration in solution, while the other was produced via oximation with an organomercury aldehyde on a solid support. These two oligonucleotide conjugates functioned as sequence-specific aRNases. The reactions conducted in the presence of mercury (II), an arylmercury complex, or the two organomercurated aRNases, exhibited considerable rate accelerations compared to reactions in the absence of any catalyst.

KEYWORDS: Oligonucleotide, hydrolysis, organometallic, mercury, catalysis, phosphodiester, cleavage, artificial ribonucleases, RNA

TURUN YLIOPISTO
Matemaattis-luonnontieteellinen tiedekunta
Kemian laitos
Kemia
LANGE YAKUBU SALEH: Organometalliset oligonukleotidit keinotekoisina
ribonukleaaseina
Väitöskirja, 88 s.
Eksaktien tieteiden tohtoriohjelma
Toukokuu 2024

TIIVISTELMÄ

Antisense-oligonukleotidit (ASOt) hyödyntävät RNaasi H:n luonnolista katalyyttistä aktiivisuutta aiheuttaakseen haluttujen RNA-sekvenssien pilkkoutumisen. ASOn soluun tunkeutumisen, pysyvyyden ja sitoutumisaffiniteetin kannalta tarpeellisten kemiallisten muutosten tekeminen vaarantamatta kykyä aktivoida RNaasi H on kuitenkin usein haastavaa. Tämä herkkä tasapaino rajoittaakin usein parhaiden mahdollisten terapeuttisten tulosten saavuttamista. Keinotekoiset ribonukleaasit (aRNaasit) on suunniteltu pilkkomaan RNA-sekvenssejä selektiivisesti, jäljitellen luonnollisten ribonukleaasien toimintaa mutta räätälöitynä haluttua sovellusta varten. Nämä synteettiset vastineet pilkkovat tehokkaasti RNA:n fosfodiesteri-sidoksia, mahdollistaen monia sovelluksia kuten halutun RNA-sekvenssin hajotta-misen solujen sisällä.

Parhaat nykyisistä aRNaaseista perustuvat metalli-ionien, kuten Cu(II) tai Zn(II), koordinaatiokomplekseihin, mikä tekee niiden käytöstä esimerkiksi solun sisällä vallitsevissa hyvin laimeissa ja metalliköyhissä olosuhteissa haastavaa. aRNaasit, joissa katalyyttinen metalli-ioni on sitoutunut hiileen, eivät dissosioidu edes äärimmilleen laimennettuna ja voisivat näin ollen yhdistää orgaanisten yhdisteiden pysyvyyden ja metallikompleksien katalyyttisen tehon. Valitsimme katalyyttiseksi metalli-ioniksi Hg(II):n, koska aryylielohopeayhdisteet ovat hydrolyyttisesti pysyviä ja helposti saatavilla.

Tämä väitöstutkimus sisältää laajalla pH-alueella tehtyjä kineettisiä mittauksia Hg(II):n ja erään aryylielohopeakompleksin katalysoimalla RNA-malliyhdiste ade-nylyyli-3´,5´-(2´,3´-O-metyleeniadenosiinin) pilkkoutumisella. Molemmat reagens-sit katalysoivat malliyhdisteen pilkkoutumista. Lisäksi syntetisoitiin vakiintuneita menetelmiä hyödyntäen kaksi oligonukleotidikonjugaattia, joilla oli sama sekvenssi mutta 5´-päässä erilainen organoelohopearyhmä. Yksi konjugaatti valmistettiin suo-ralla merkuraatiolla liuoksessa ja toinen oksimaatiolla organoelohopea-aldehydin kanssa kiinteällä kantajalla. Molemmat olikonukleotidikonjugaatit toimivat sekvens-sispesifisinä aRNaaseina. Sekä Hg(II):n, aryylielohopeakompleksin että organo-elohopea-aRNaasien läsnä ollessa suoritetut reaktiot olivat huomattavasti nopeampia kuin vastaavat reaktiot ilman katalyyttiä.

ASIASANAT: Oligonukleotidi, hydrolyysi, organometallinen, elohopea, katalyysi, fosfodiesteri, pilkkominen, keinotekoiset ribonukleaasit, RNA

Table of Contents

Abbreviations

A	adenine
AAV	adeno-associated virus
AGO	antigene oligonucleotide
aRNase	artificial ribonuclease
ASO	antisense oligonucleotide
Bz	benzoyl
C	cytosine
CPPs	cell-penetrating peptides
DMF	dimethylformamide
DMTr	4,4′-dimethoxytrityl
DNA	deoxyribonucleic acid
ds	double-stranded
FDA	U.S. Food and Drug Administration
G	guanine
glmS	glucosamine-6-phosphate synthase
HDV	hepatitis delta virus
IE-HPLC	ion exchange-high performance liquid chromatography
LNA	locked nucleic acid
lncRNA	long non-coding RNA
miRNA	microRNA
MOE	methoxyethyl
mRNA	messenger RNA
MS	mass spectrometry
NMR	nuclear magnetic resonance
ON	oligonucleotide
PMOs	phosphorodiamidate morpholino oligomers
PNA	peptide nucleic acid
pre-miRNA	precursor miRNA
pri-RNA	primary RNA
PS	phosphorothioate
RISC	RNA-induced silencing complex

RNA	ribonucleic acid
RNase H	ribonuclease H
RNase P	ribonuclease P
RP-HPLC	reversed phase-high performance liquid chromatography
RP-UPLC	reversed phase-ultra performance liquid chromatography
rRNA	ribosomal RNA
SELEX	Systematic Evolution of Ligands by EXponential enrichment
S_N2	bimolecular nucleophilic substitution
ss	single-stranded
SSO	splice switching oligonucleotide
T	thymine
$t_{1/2}$	half-life
TBDMS	*tert*-Butyldimethylsilyl
THF	tetrahydrofuran
TLC	thin-layer chromatography
T_m	melting temperature
tRNA	transfer RNA
TsCl	*p*-Toluenesulfonyl chloride
U	uracil
UpU	uridylyl-3´,5´-uridine
VS	Varkud satellite

List of Original Publications

This dissertation is based on the following original publications, which are referred to in the text by their Roman numerals:

I   **Lange Yakubu Saleh**, Mikko Ora, Tuomas Lönnberg, "Mercury(II)-Catalyzed Cleavage, Isomerization and Depurination of RNA and DNA Model Compounds and Desulfurization of Their Phosphoromonothioate Analogs," *Catalysts*, 2020; 10:219.

II   **Lange Yakubu Saleh**, Mikko Ora, Tuomas Lönnberg, "Cleavage of an RNA Model compound by an Arylmercury complex," *ChemBioChem*, 2021; 10: 1761–1764.

III   **Lange Yakubu Saleh**, Mikko Ora, Tuomas Lönnberg, "Organomercury oligonucleotide conjugates as artificial ribonucleases," *Journal of Inorganic Biochemistry*, 2023; 247: 112331

The original publications have been reproduced with the permission of the copyright holders.

List of other related publications

I   Tharun K. Kotammagari, **Lange Yakubu Saleh**, Tuomas Lönnberg, "Organometallic modification confers oligonucleotides new functionalities" *Chem. Commun.,* 2024; 60:3118–3128

1 Introduction

1.1 General Background

The Introduction provides an overview of RNA & DNA, encompassing their structures and roles. Subsequently, it delves into challenges and solutions in oligonucleotide therapeutics, discussing the main modalities. Following that, it examines various RNA phosphodiester bond cleavage mechanisms. Finally, the section most closely related to the thesis focuses on artificial ribonucleases, exploring four key design strategies and the three essential components.

1.1.1 Structure of RNA & DNA

DNA (deoxyribonucleic acid) and RNA (ribonucleic acid) are fundamental biopolymers that play critical roles in storing, transmitting, and expressing genetic information within living organisms. These nucleic acids are composed of nucleotides, which serve as the building blocks for their structures.

DNA is formed of two strands of nucleotides that intertwine to create a double helix structure. Each nucleotide consists of a sugar molecule, a phosphate group, and a nitrogenous base (adenine A, cytosine C, guanine G, or thymine T). The linkage between nucleotides occurs through a phosphodiester bond, where the 5′ carbon of one nucleotide connects to the 3′ carbon of the next. The sugar and nucleobase are joined through an *N*-glycosidic bond, *via* N9 in purines and N1 in pyrimidines. The base pairs between the two DNA strands are held together by hydrogen bonds, A pairing with T and G with C. This complementary base pairing is referred to as Watson—Crick base pairing (Figure 1). The specific sequence of these base pairs determines the genetic information encoded in DNA. RNA exhibits a similar structure to DNA, but it is typically single-stranded (ss) and contains the nitrogenous base uracil U instead of T. Additionally, RNA utilizes ribose sugar instead of the deoxyribose sugar present in DNA.

1.1.2 Biological roles of RNA & DNA

In the realm of genetic information transfer, the central dogma theory suggests the flow of information from DNA to protein via RNA. Within this process, various

types of RNA each perform crucial functions such as messenger RNA (mRNA) encoding proteins, transfer RNA (tRNA) loading amino acids, and ribosomal RNA (rRNA) assembling the protein. However, the significance of RNA extends beyond these well-established roles, as it plays a central part in diverse cellular regulatory pathways.[1] During transcription, the genetic information stored in DNA is copied into a complementary RNA molecule. Additionally, DNA is involved in regulating gene expression, determining which genes are active and when, through mechanisms like the binding of regulatory proteins, histone modification, and chemical group modification of the DNA molecule.[1,2]

Non-coding RNAs do not encode proteins but serve various regulatory functions within the cell. Examples of non-coding RNAs include tRNA, rRNA, microRNA (miRNA), and long non-coding RNA (lncRNA). Recent research has highlighted the diverse and critical roles of non-coding RNAs in shaping cellular activity and diagnostics.[3] miRNAs, for instance, have been found to regulate gene expression, while lncRNAs have been associated with processes like chromatin organization and gene regulation.[4]
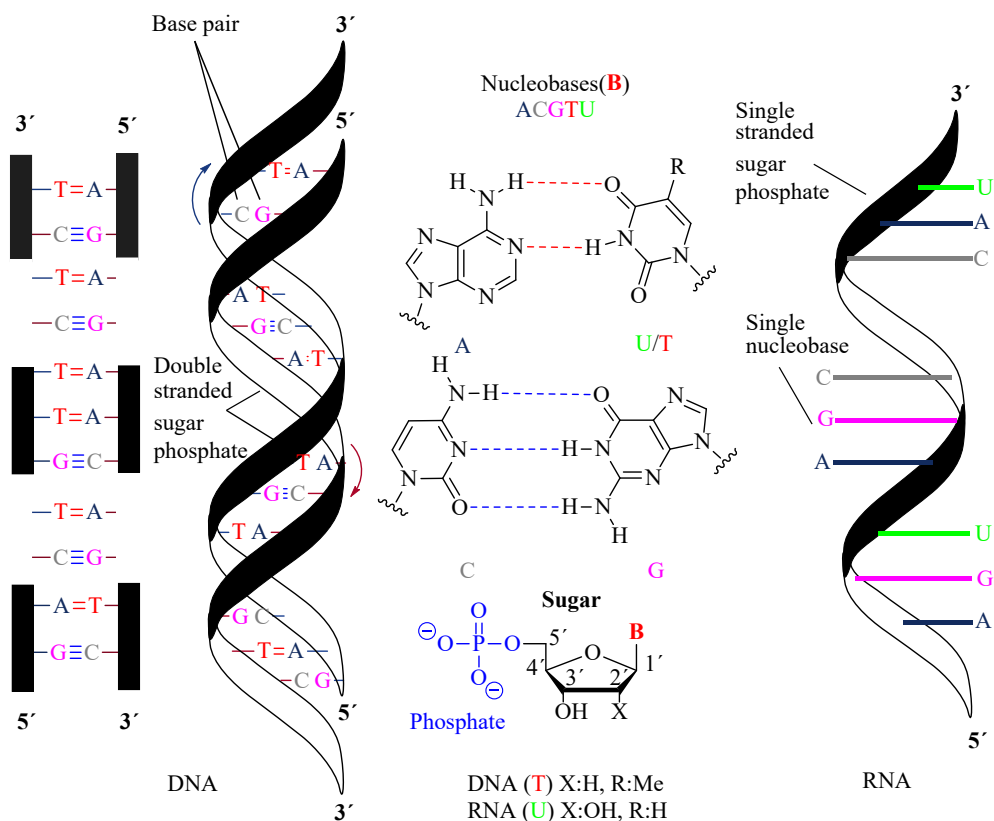

Figure 1. The canonical structures and Watson-Crick base pairing in DNA and RNA.

1.2   Oligonucleotide therapeutics

In 1978, Zamecnik and Stephenson[5] demonstrated the inhibitory effect of oligonucleotides (ONs) on viral replication in a laboratory setting. Since then, extensive research has been carried out to realize the therapeutic potential of ONs in targeting mRNA and other nucleic acids for the treatment of various diseases.[6]

A notable characteristic of the human genome[7] is that sequences of 17 nucleotides or more statistically occur only once. This unique property enables precise binding of ON therapeutics to their intended targets. Such selective binding is crucial for the therapeutic effectiveness of ONs targeting DNA (Antigene oligonucleotides (AGOs)) or RNA (microRNAs (miRNAs), splice switching oligonucleotides (SSOs), and antisense oligonucleotides (ASOs)). Among these, ASOs can be classified into two primary types: those that promote RNA degradation and those that inhibit RNA function. Aptamers, which target disease-related proteins, undergo self-hybridization, forming complex folded structures.

Although ON therapeutics hold tremendous potential, their usage necessitates addressing certain challenges and concerns.[8]

1. Delivery: Presently, intravenous injection serves as the predominant method, but it has drawbacks such as restricted exposure to target cells and swift elimination from the body. To surmount these limitations, researchers are actively exploring alternative delivery approaches. These include employing liposomes or nanoparticles by conjugating them with ASOs, directly injecting ASOs into target tissues, and employing adeno-associated virus (AAV) vectors.[9] Additionally, conjugates such as peptide nucleic acids or cell-penetrating peptides have shown potential in improving the cellular uptake and activity of ASOs.

2. Specificity: ONs can bind to unintended RNA sequences, which can cause off-target effects and diminish their specificity. This unintended binding may inhibit crucial genes, leading to undesirable side effects. To enhance specificity, scientists are investigating the potential of chemically modified ASOs, such as locked nucleic acid (LNA), which exhibit heightened binding affinity towards the intended target RNA sequences.[10]

3. Immune Response: The body may initiate an immune response against ONs, diminishing their efficacy over time. This phenomenon has been observed during clinical trials investigating ONs as potential treatments for specific genetic disorders. Modifying the backbones of ONs through chemical alterations, such as incorporating phosphorothioate (PS), methoxypropylphosphonate (MOP), mesyl phoshoramidate (MsPA), and/or introducing sugar modifications like LNA, 2′-(methoxyethyl) (2′-MOE), 2′-O-methyl (2-OMe), 2′-Fluoro (2′-F), and bridged nucleic acid (BNA), has proven instrumental in reducing immunogenicity.[11]

4. Stability: One crucial factor when it comes to ONs is their degradation within the body, which can lead to decreased effectiveness. To overcome this challenge, various chemical modifications have been applied to ONs in their backbone and sugar structures, including PS, MOP, MsPA, 2′-OMe, LNA, BNA,[12] MOE, 2′-F, PMO and PNA. These modifications have demonstrated heightened stability and improved pharmacokinetic properties, ultimately enhancing the overall efficacy.[13]

5. Complexity: Treating diseases that stem from multiple genetic factors or possess intricate pathophysiology necessitates more than just targeting a single gene. In such instances, a combination therapy involving multiple ASOs may be necessary for effective treatment.[14]

Applicable chemical modifications[15] vary depending on the modality as a certain type of modification could either increase or reduce the levels of resistance to the enzyme RNase H, binding affinity, renal clearance, and cytotoxicity.[16]

1.2.1 Antisense Oligonucleotides (ASOs)

ASOs are short, chemically synthesized RNA or DNA molecules designed to hybridize with complementary mRNA sequences. They serve the purpose of inhibiting the expression of particular genes by binding to the target mRNA, preventing its translation into proteins (Scheme 1). ASOs have found applications in various fields, including the treatment of infectious diseases, cancer, and genetic disorders.[17–19] The first antiviral ASO was Vitravene (fomivirsen), developed to treat cytomegalovirus retinitis in immunocompromised patients, including those with AIDS. Another example is Tegsedi (Inotersen), which is employed for the management of hereditary transthyretin amyloidosis — a condition characterized by the accumulation of amyloid proteins in the organs and tissues of the body.
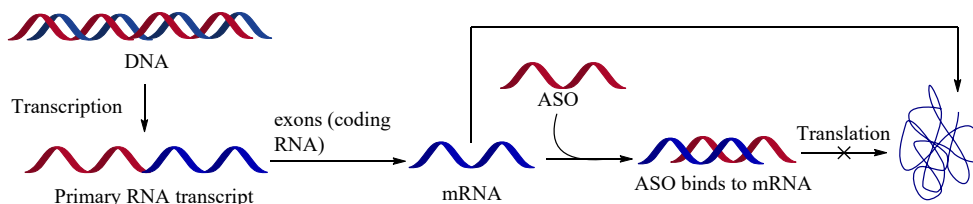
Scheme 1. Mechanism of action for ASOs.

ASOs can recruit an enzyme called RNase H, which plays a role in cleaving RNA within a hybrid RNA–DNA duplex. RNase H can be hindered by certain modifications in ASOs, causing reduced or lost activity. For instance, 2′-OMe groups disrupt the RNA–DNA hybrid structure which may impair RNase H cleavage. PS backbone modifications, while enhancing stability, can also interfere

with RNase H activity, especially when excessively applied. LNA modification may boost binding affinity but might reduce RNase H activity since it involves locking the sugar in a C3´-endo conformation. Bulky modifications causing steric hindrance can block RNase H access. The impact of modifications varies based on ASO location, target RNA, and design.

ASOs that are either too short or too long may not effectively activate RNase H. Typically, ASOs ranging from 15–25 nucleotides in length exhibit the best RNase H activation. Another factor affecting ASO efficiency is the specific binding site within the target mRNA. Binding sites located in particular regions, such as the 5´ untranslated region or the coding region, tend to be more effective at activating RNase H than binding sites in other regions.[20,21]

1.2.2   Splice Switching Oligonucleotides (SSOs)

SSOs are short sequences typically consisting of 15–30 nucleotides. They are designed to bind to pre-mRNA in order to disrupt RNA-RNA/protein interactions and evade the spliceosome, thereby affecting the recognition of splice sites (Scheme 2). When an SSO pairs with an RNA target and alters the spliceosome's recognition of the cleavage site, it leads to a modification in the splicing process of the targeted transcript. The RNase H-resistant properties of SSOs[22] are crucial, as their purpose is to modulate splicing rather than to degrade the pre-mRNA. Recently approved SSOs include Viltepso and Amondys 45 that are used to treat Duchenne Muscular Dystrophy. A number of chemical modifications[22,23] have been studied to improve the therapeutic potential of SSOs. PS backbone modification increases SSO stability and nuclease resistance, while 2´-OMe, 2´-MOE, LNA and PNA modifications enhance binding affinity and specificity. Morpholino modification is known for its high specificity for RNA targets, resistance to nucleases and inability to activate RNAse H. Other backbone modifications like amide or phosphorodiamidate have
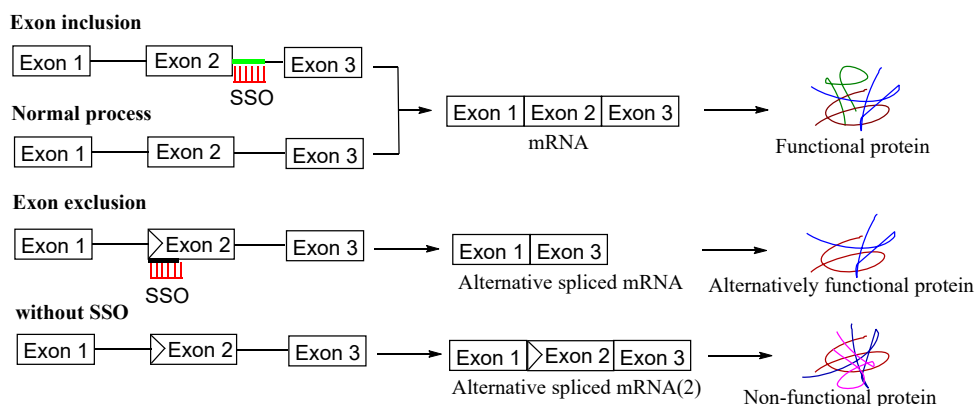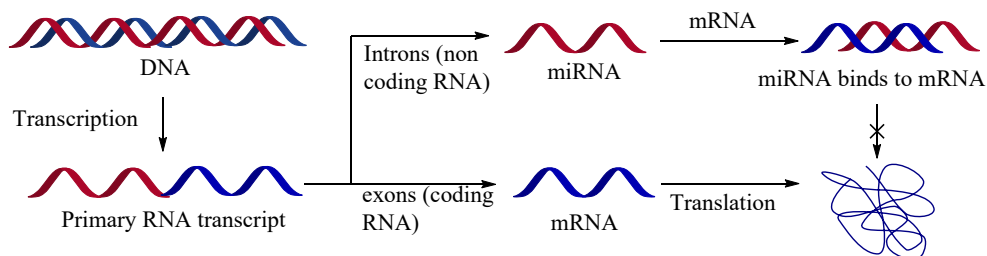

Scheme 2. Mechanism of actions for SSOs.

also been explored. Chimeric SSOs, combining different modifications offer a balance between stability, affinity, and specificity. The potential off-target effects have to be considered when optimizing SSOs for therapeutic or research applications.[22,24]

1.2.3 MicroRNAs (miRNAs)

miRNAs are short RNA molecules, typically consisting of 18–24 nucleotides, that play a crucial role in regulating gene expression.[25] Unlike coding RNA, miRNAs do not encode proteins and are hence classified as non-coding RNA. One mechanism by which miRNAs exert their control is by binding to complementary sequences within mRNA molecules, thereby inhibiting protein translation and reducing the expression of the targeted gene. The production of miRNAs (Scheme 3) involves transcription from DNA sequences, leading to the formation of primary RNA (pri-RNA). Subsequently, this pri-RNA undergoes processing into precursor miRNA (pre-miRNA), which ultimately matures into functional miRNA through a series of enzymatic cleavage events. Although numerous animal miRNAs have been identified, only a small fraction of them[26] have been linked to specific mRNA targets due to the limited pairing involved. miRNAs have diverse functions in biological processes such as cell proliferation, apoptosis, development, and differentiation.

Scheme 3. Mechanism of actions for miRNAs.

Furthermore, they have been implicated in diseases including cancer and viral infections. Notably, miRNAs are not limited to animals; they are also found in plants and various viruses. The potential therapeutic applications of miRNAs have attracted considerable interest in the scientific community, although no approach for clinical practice has been firmly established.[27]

1.2.4 Antigene Oligonucelotides (AGOs)

AGOs are synthetic DNA or RNA molecules designed to specifically target and block the expression of particular genes. In contrast to ASOs, they achieve this by

binding directly to DNA[28] itself through formation of a triple helix. Furthermore, AGOs can induce a permanent and heritable disruption of gene expression and function, providing long-term therapeutic effects. AGOs are typically longer than ASOs, ranging from 15–35 nucleotides in length. Longer ONs generally have stronger binding affinity but also a higher probability of off-target effects. Unlike ASOs, which rely on Watson-Crick hydrogen-bonding interactions, AGOs employ a different mechanism called Hoogsteen or reverse Hoogsteen base pairing. This mechanism (Scheme 4) specifically targets sequences with homopyrimidine–homopurine compositions.[28,29]
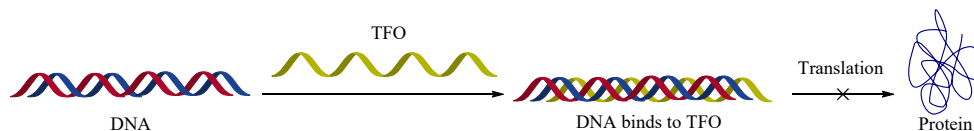
Scheme 4. Mechanism of actions for AGOs.

AGOs show significant promise as a tool for selectively inhibiting gene expression, with potential applications in various disease processes such as cancer and viral infections. However, further research is necessary to optimize their delivery and minimize off-target effects, ensuring their safe and effective use in clinical settings.

1.2.5 Aptamers

Aptamers are artificial, single stranded oligonucleotides that typically consist of 30–80 nucleotides. By adopting specific three-dimensional structures, aptamers can effectively bind to a diverse range of targets, including small molecules, proteins, and cells (Scheme 5). Aptamers are derived from a large pool of random sequences using a process called SELEX (Systematic Evolution of Ligands by EXponential Enrichment). During SELEX[30] aptamers with the highest affinity for the target molecule are selected and amplified, resulting in a collection of high-affinity aptamers. In various applications such as diagnostics, drug discovery, food science, drug transport, and therapies, aptamers are often utilized as an alternative to antibodies.[31,32]
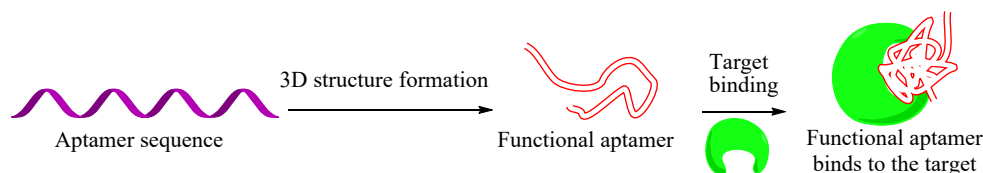
Scheme 5. Mechanism of actions for Aptamers.

Over the past two decades, aptamer therapies have undergone numerous trials and improvements, providing a wide array of potential therapeutic applications. Notably, in 2004, the US FDA approved the first aptamer-based therapeutic, Macugen (pegaptanib), for treating age-related macular degeneration. This aptamer specifically targets vascular endothelial growth factor. Despite their promise, aptamers, like all unmodified oligonucleotides,[33] are susceptible to rapid degradation by nucleases within the body and clearance via glomerular filtration, resulting in a short half-life.

1.2.6 Chemical modifications vs. reliance on endogeneous enzymes for RNA cleavage

The involvement of cellular machinery (RNase H and RISC complex)[34] in RNA cleavage plays a vital role in gene regulation and resistance against foreign genetic material. Increasing the potential of oligonucleotide therapeutics through chemical modifications[15] faces limitations when one of these mechanisms is involved. [14] To address this issue, there is a growing demand for artificial ribonucleases capable of cleaving RNA independently of cellular machinery. The development of artificial ribonucleases requires a thorough understanding of the functions of natural ribonucleases and the impact of oligonucleotide modifications on these processes.

1.3   Cleavage of RNA Phosphodiester Bonds

RNA phosphodiester bond cleavage is at least a million times faster compared to DNA.[35–37] This disparity is attributed to the presence of the 2′-OH group in RNA, which acts as an intramolecular nucleophilic catalyst. In contrast, the 2′-H group in DNA lacks catalytic properties.

The mechanism of RNA hydrolysis[38] (Scheme 6) involves the attack of the 2′-OH group on the phosphorus atom. This attack leads to the formation of a pentacoordinated phosphorane intermediate. Depending on the departing oxygen
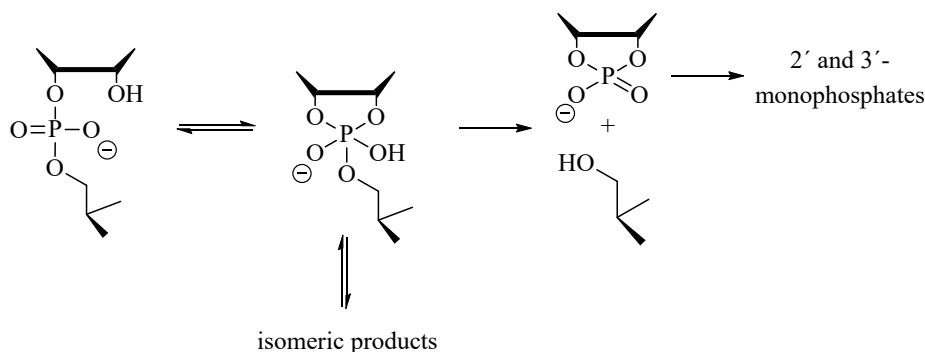
isomeric products

Scheme 6. Hydrolysis of an RNA phosphodiester bond.

atom, the reaction can yield the 3´,5´-isomer, 2´,5´-isomer, or the cleaved products. The cleaved products consist of a nucleoside and a terminal 2´,3´-cyclic monophosphate, which is an unstable intermediate and eventually breaks down to a 2´- or 3´-monophosphate.

The pseudorotation theory, initially proposed by Westheimer in the 1960s, provides an explanation for the product distribution of transesterification of RNA phosphodiester linkages (Scheme 7).[39] According to this theory, the process involves a pentacoordinate phosphorane intermediate that undergoes stereomutation through pseudorotation. Let's delve into the theory in more detail:

1. When a nucleophile attacks a tetrahedral phosphorus, it leads to the formation of a phosphorane molecule with a trigonal bipyramidal geometry, which possesses five ligands.
2. The orientation of these ligands can be either equatorial or apical. The phosphorane has the ability to reorganize through a process known as pseudorotation, wherein two of the equatorial ligands become apical, while one ligand retains its equatorial position. It is important to note that this rearrangement occurs only if the phosphorane is an actual intermediate and not merely a transition state.
3. Nucleophiles can enter and exit the phosphorane solely through the apical sites. This principle is referred to as the extended principle of microscopic reversibility.
4. The specific positioning of certain substituents can influence the preference for apical or equatorial sites in different scenarios. Here are a few examples:
    *   A four- or five-membered ring prefers to be attached in apical/equatorial orientation to the central atom.
    *   Ligands with higher electronegativity tend to favor apical positions.
    * π electron donors typically prefer equatorial positions.
    *   Sterically bulky substituents mostly favor equatorial positions.
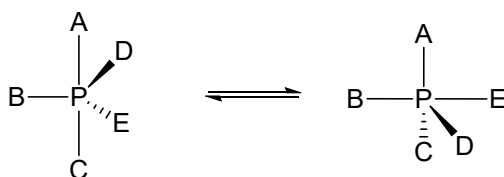
Scheme 7. Pseudorotation of a pentacoordinated phosphorane.

1.3.1 Spontaneous hydrolysis

Spontaneous hydrolysis is the degradation of phosphodiester bonds within RNA molecules, occurring without the need for external catalysts. At 25 °C, the half-life ($t_{1/2}$) of RNA spontaneous hydrolysis is approximately 4 years.[40–44] Spontaneous hydrolysis is pH-independent and can be observed only within a narrow pH range centered around pH 5. Under these conditions, isomerization occurs approximately 20 times faster.[43] Spontaneous hydrolysis serves as a critical reference point for other types of reactions, making it significant despite its slow rate. The mechanism underlying this process is demonstrated in Scheme 8. The reaction initiates with a proton transfer from the 2′-OH to the monoanionic phosphorane, followed by the attack of the 2′-oxyanion on the neutral phosphate, resulting in the formation of a cyclic monoanionic phosphorane. Subsequently, the intermediate undergoes breakdown into a nucleoside and a terminal 2′,3′-cyclic monophosphate. These products can then be further cleaved into either a 2′- or a 3′-monophosphate.
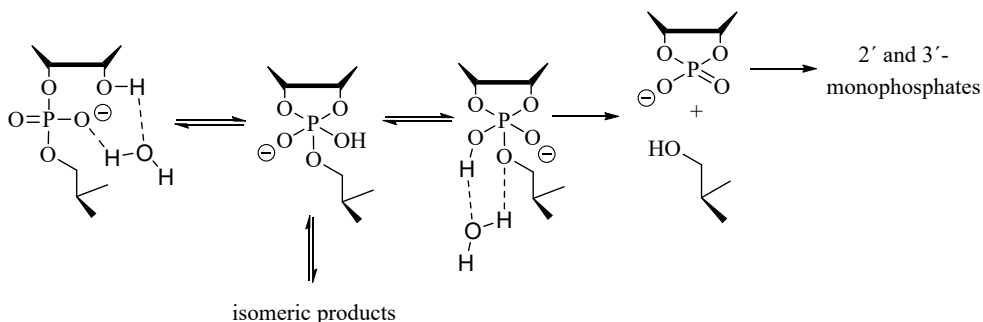
Scheme 8. Spontaneous hydrolysis of RNA phosphodiester bond.

1.3.2 Specific base catalyzed hydrolysis

When the pH exceeds 7.5, specific base[38,45,46] catalyzed hydrolysis becomes the dominant mechanism. Under basic conditions, only the cleavage reaction takes place. It involves the rapid deprotonation of the 2′-OH group, followed by the attack of the resulting 2′-oxyanion on the phosphorus atom (Scheme 9). The resulting dianionic phosphorane intermediate cannot pseudorotate and instead breaks down exclusively into a cyclic monophosphate and a ribonucleoside 5′-oxyanion.
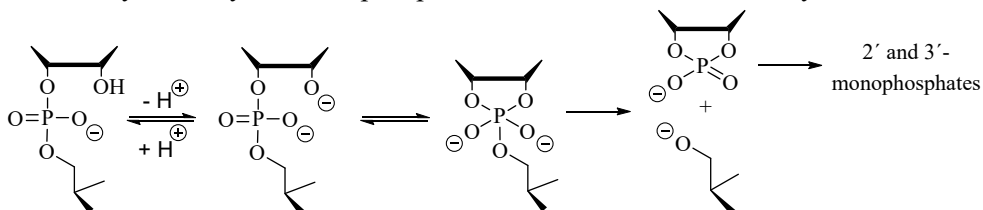

Scheme 9. RNA hydrolysis by specific base.

1.3.3   Specific acid catalyzed hydrolysis

Under acidic conditions, two processes occur: the cleavage of the 5′-linked nucleoside and the isomerization between 3′,5′- and 2′,5′-phosphodiesters. The mechanism of specific acid catalyzed hydrolysis involves the protonation of one or both of the non-bridging oxygen atoms in the phosphate group. Consequently, the phosphate undergoes an attack by the 2′-OH, resulting in the formation of an unstable intermediate, which is capable of undergoing pseudorotation to yield an isomeric product (2′,5′-isomer). Subsequently, this intermediate eventually decomposes into a cyclic monophosphate and a ribonucleoside.

   At pH below 1, the phosphodiester bond is in a monoprotonated neutral state while the reactive form is the monocation, resulting in a first-order dependence on hydronium ion concentration.[43] Above pH 1, the dominant form is the monoanionic phosphodiester and the reaction rate depends on hydronium ion concentration in a second-order manner. The monocationic phosphorane obtained through attack of the 2′-OH (Scheme 10) can become neutral and pseudorotate, leading to P-O3′ or P-O5′ bond cleavage depending on which oxygen is protonated. This aligns with experimental findings indicating similar rates of isomerization and phosphodiester cleavage.[43]
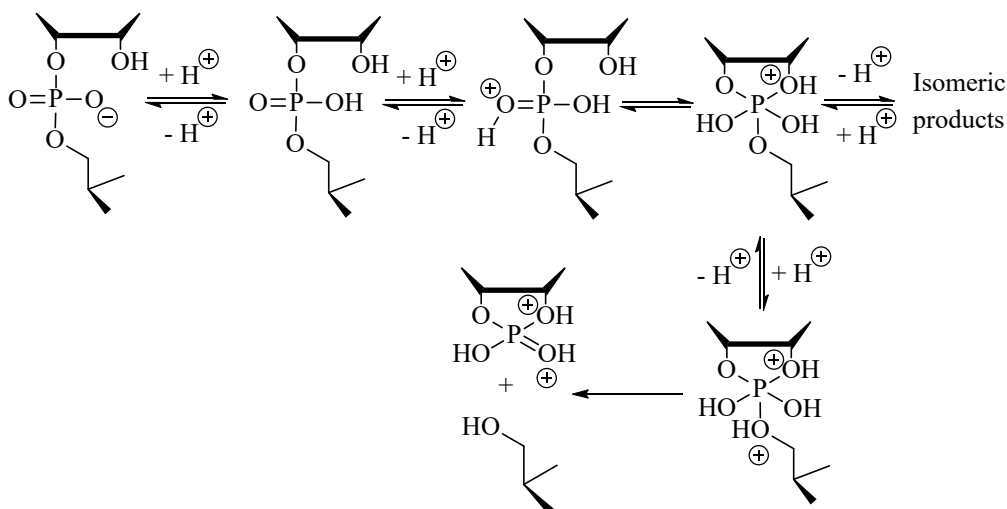
Scheme 10. Specific acid catalyzed hydrolysis involving a monocationic phosphodiester bond.

   At around pH 3, the reaction again becomes first-order in hydronium ion concentration. In this scenario, the primary reaction pathway involves the attack of the 2′-OH (Scheme 11) on the neutral phosphate, which is obtained after the rapid protonation of the monoanion. Another possible description of the mechanism involves the formation of a phosphorane from a minor tautomer, where the phosphate

is protonated, and the *2′-O* is deprotonated, followed by an acid-catalyzed breakdown. Kinetically, these two mechanisms are indistinguishable.[43,47]
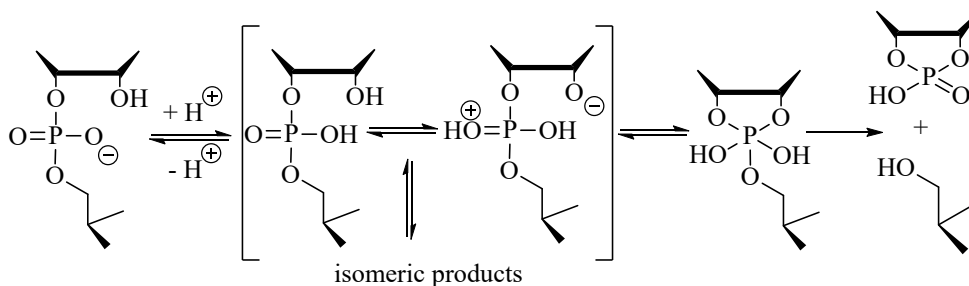
Scheme 11. Specific acid catalyzed hydrolysis involving a neutral phosphodiester bond.

1.3.4 General acid/base catalyzed hydrolysis

RNA phosphodiester bonds can undergo cleavage through general acid/base–catalyzed reactions, although the efficiency of such reactions is limited. Buffer catalysis for the isomerization reaction is often too weak to be quantified reliably. In relatively alkaline buffers, catalysis by only the basic buffer component is observed (Scheme 12). Two kinetically equivalent interpretations are possible. The first one involves deprotonation of the attacking 2′-OH group catalyzed by a general base, along with a more or less concerted breakdown of the dianionic phosphorane (Scheme 12A). The second one involves the general acid catalyzed breakdown of the dianionic phosphorane obtained by attack of 2′-oxyanion on negatively charged phosphate (Scheme 12B). In more alkaline buffers, and with ribonucleoside 3′-phosphodiesters that have a better leaving group, the former reaction predominates over the latter.

With the less alkaline imidazole and morpholine buffers, both the acidic and basic components are catalytically active.[48–50] The proposed mechanism (Scheme 12C) involves the formation of a monoanionic phosphorane intermediate catalyzed by a specific acid/general base (where the phosphate is protonated by a specific acid, and the 2′-OH is deprotonated by a general base), followed by specific base/general acid breakdown (where the specific base deprotonates the phosphate and a general acid facilitates the departure of the 5′-leaving group by providing a proton).
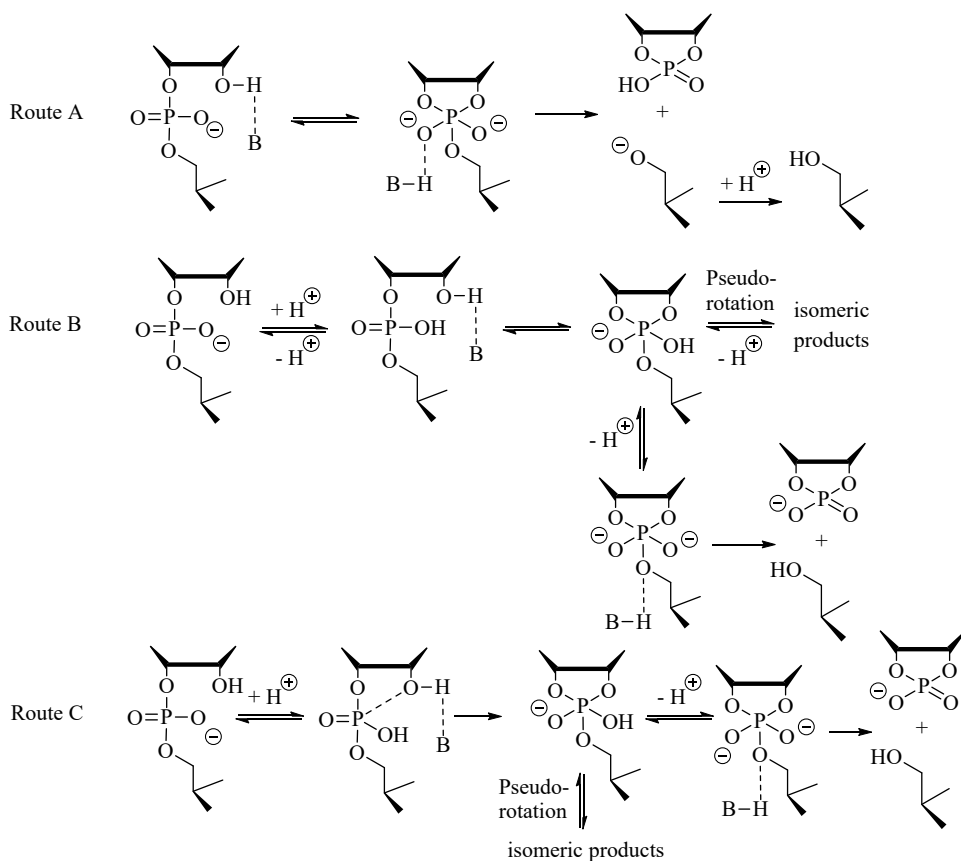
Scheme 12. Buffer-catalyzed hydrolysis in RNA phosphodiester bonds.

1.3.5   Metal ion catalysis

Metal ions, particularly divalent ones, play a crucial role in their interaction with RNA[51,52] serving to shield negative charges and thus stabilize regions with multiple phosphates. While monovalent cations can also fulfill this function, divalent metals are more effective in certain RNA structures like ribozymes. Binding of metal ions to specific sites on RNA is essential for maintaining its structure and facilitating its functions. Water molecules play a vital role in mediating interactions between nucleic acid molecules and metal ions.[52] In addition to providing structural stability, metal ions also act as catalysts and co-catalysts in ribozymes.[53]

There is no one universally accepted catalysis mechanism but several, depending on the metal ion. However, there is a consensus regarding the importance of proton transfer events occurring at a pH close to the pK_a of a metal-bound water molecule. Four distinct mechanisms[37,54–57] have been proposed. Schemes 13A and 13C represent nucleophilic and electrophilic catalysis, where the metal ion serves a dual

role of enhancing the nucleophilicity of 2´-OH group by promoting its deprotonation, and also increasing the electrophilicity of the phosphate through coordination. The mechanisms depicted in Schemes 13B and 13D involve general acid-base catalysis by aqua or hydroxo ligands of a metal ion coordinated to the oxygen atoms of the scissile phosphodiester bond. The metal hydroxo ligand serves as a general base, facilitating attack of the 2´-OH by deprotonation. A metal-bound water molecule may stabilize the negative charge in the transition state and facilitate the departure of the leaving group as a general acid.

Lanthanide ions[58,59] Eu(III), Tb(III), La(III), and Yb(III) exhibit remarkable catalytic prowess in the cleavage of RNA phosphodiester bonds, achieving a rate enhancements of three to four orders of magnitude compared to the uncatalyzed reaction. Other heavy metal ions, such as Zn(II), Pb(II), and Cu(II) typically exhibit lower but in many cases still useful activity.[60] For instance, Zn(II) demonstrates approximately 4% of the catalytic activity observed with Pb(II), while other ions such as Mg(II), Cd(II), Cu(II), or Mn(II) exhibit significantly slower[61] rates.
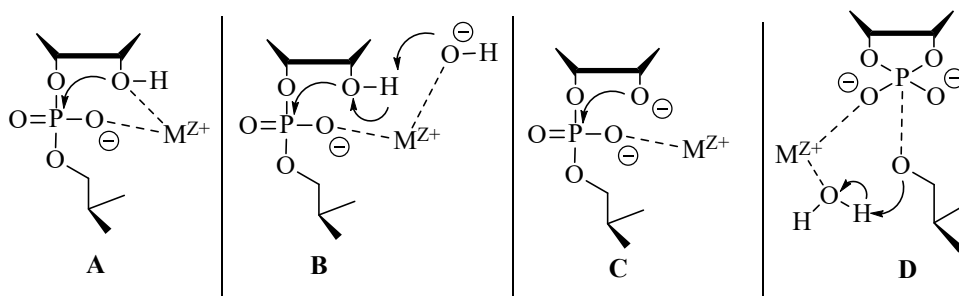
Schme 13. Alternative approaches for the cleavage of phosphodiesters facilitated by metal ions.

1.3.6 Enzyme catalysis

Enzyme catalysis plays a vital role in accelerating biochemical reactions. Multiple enzymes facilitate the cleavage of phosphodiester bonds.[62] Research has focused on investigating the catalytic properties of various small molecules to gain a better understanding of how enzymes facilitate RNA processing reactions.[37,38] These studies have also been driven by the goal of developing artificial ribonucleases.[63] The catalytic process employed by enzymes[64] exemplified by RNase A (Scheme 14), involves transphosphorylation between the 2´-OH group of a ribose and its vicinal phosphodiester group. RNase A employs a general acid/base mechanism facilitated by two histidine residues: histidine 12 functions as a general base, deprotonating the 2´-OH group of the substrate RNA, while lysine 41 offers electrostatic stabilization to support the accumulation of negative charge in the pentacoordinate phosphorane intermediate. Furthermore, histidine 119 donates a

proton to the 5´-oxygen of the 3´ nucleoside. This protonation step enhances the removal of the 5´-leaving group and facilitates the $S_N2(P)$-like "in-line" attack by the 2´-oxygen.
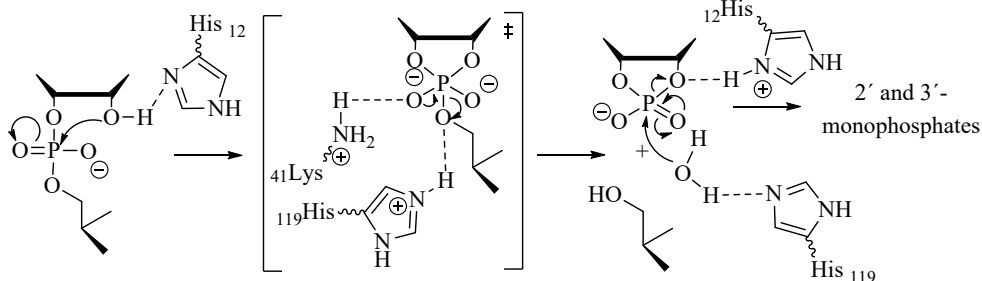
Scheme 14. Enzyme hydrolysis of RNA phosphodiester bond.

1.3.7   Ribozyme catalysis

The groundbreaking discovery by Cech and Altman revealed the crucial role of RNA molecules in catalyzing essential processes within cells. Through *in vitro* studies, it has been demonstrated that engineered ribozymes can catalyze both non-biological[65] and biological reactions.[66] Nature has provided us with various well-known categories of ribozymes, including small self-cleaving ribozymes[67] like hatchet, glucosamine-6-phosphate synthase (glmS), hammerhead, hepatitis delta virus (HDV)-like, hairpin, pistol, Neurospora Varkud satellite (VS), twister, twister sister, as well as recently discovered hovlinc and mammalian SINE ribozymes. These small ribozymes,[67–69] ranging from 50 to 150 nucleotides in length, are mainly found in plant viral RNA satellites and play vital roles in viral RNA replication, splicing, and transfer RNA biosynthesis. It is noteworthy that most ribozymes cleave between base-paired regions, resulting in products with lower affinity for the ribozyme compared to the substrate. Conversely, larger ribozymes,[70,71] such as Group I and II introns and ribonucleoprotein (RNase P), consist of hundreds of nucleotides and exhibit similar catalytic functions as small ribozymes but differ in their mechanism.[70,72,73] The hydrolysis mechanism observed in small ribozymes closely resembles the non-enzymatic hydrolysis of RNA. Large ribozymes, in turn, initiate their action when an external nucleophile attacks a 3´,5´-phosphodiester bond. This external nucleophile can take the form of the 3´-OH group from an external nucleoside, a water molecule, or even the 2´-OH group of another nucleoside located distantly within the same strand. The presence of Mg(II) ions is typically crucial for achieving optimal catalytic activity.

1.4 Artificial Ribonucleases

Artificial ribonucleases (aRNases)[63,74–76] are synthetic molecules that have been designed with the specific purpose of breaking the phosphodiester bonds in RNA. These engineered molecules offer a wide range of applications in biotechnology, including mRNA therapeutics and RNA sequencing. Unlike existing therapeutic approaches, particularly ASOs relying on RNase H activity, aRNases offer a solution to the limitations and challenges encountered in the field of oligonucleotide therapeutics (see section 1.2). aRNases can be classified into two groups: metal-independent[63,76] or metal-dependent, while metal dependent aRNases are further divided into two categorizes depending on whether they employ lanthanide ions[77,78] (inner transition) or divalent metal ions (transition).[79,80] Figure 2 illustrates the general design of aRNases, featuring an oligonucleotide structure connected to a
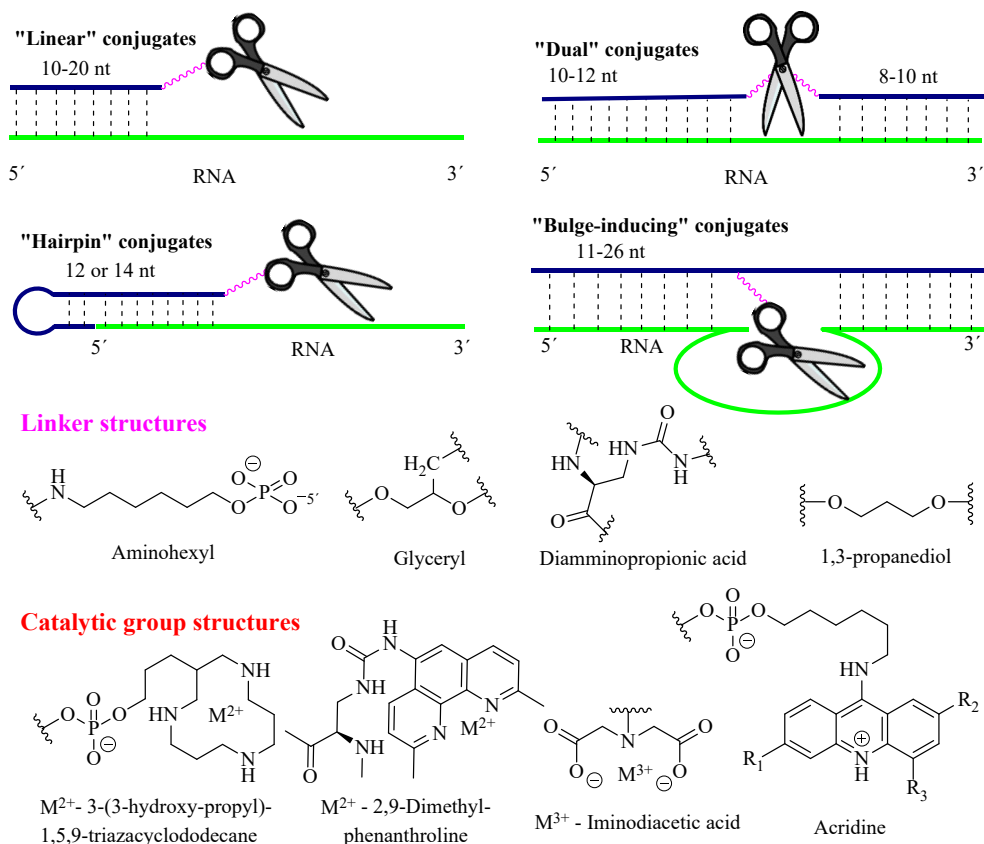

Figure 2. General representation of duplexes of aRNase having various design with RNA targets (green lines), highlighting the essential structural components: oligonucleotide recognition motifs (dark blue lines) with numbers representing their length, linkers (pink zig-zag) and catalytic domains (scissors and red).

catalytic group through a linker. The oligonucleotide architectures of aRNases can be categorized into four groups. The first category is linear conjugates,[78,81] where the catalytic moiety is attached to the 5′-terminal end of the oligonucleotide recognition motif. In dual conjugates,[82,83] the RNA recognition motif is divided into two oligonucleotide shoulders that match the 5′- and 3′-extremities of RNA targets. The catalytic moiety is positioned between them, facing a short (3–5 nucleotides) single-stranded gap formed upon hybridizing with the RNA target. Bulge-inducing ss-aRNases[84] are complementary to RNA targets that form a short (3–5 nucleotides) bulge upon hybridizing with the conjugate. The catalytic moiety of these ss-aRNases is positioned opposite the bulge. The fourth group features a hairpin oligonucleotide as an RNA recognition domain. This oligonucleotide comprises a 6- or 9-nucleotide stem and a 12–16-mer single-stranded fragment that complements the 5′-end of the target RNA, leading to enhanced binding. A hairpin near the RNA binding sequence increases duplex stability through stacking interactions[85] and significantly boosts the nuclease resistance of ss-aRNases.[86,87] Well-designed aRNases not only minimize off-target effects but also increase efficacy, ensuring a sustained and potent therapeutic impact.[63,86,88] What sets aRNases apart from natural ribonucleases is their programmable specificity for any given target sequence.[63] Moreover, certain aRNases can serve both as a standalone therapy and as adjunctive treatment in conjunction with radiotherapy, chemotherapy, and surgical interventions.[86]

1.4.1   The catalytic moiety

The catalytic moiety of an artificial ribonuclease has the ability to cleave phosphodiester bonds, mimicking the catalytic core of natural ribonucleases. The catalytic moiety[63,84,89] is situated at one end of the linker. These moieties can be broadly classified into two main types: those incorporating metal complexes[78,79] and those that are metal-independent, featuring general acid/base catalysts[90] at the catalytic core. Several metal-free moieties have been employed, with notable examples including trisbenzimidazole,[91–93] imidazoles[90] and peptides.[87,94,95] The catalytic efficiency of metal-dependent systems [77–80,88,89,96–100], encompassing both divalent and lanthanide metals, has undergone intensive investigation. Noteworthy examples of these complex cores include dimethylphenanthrolines, azacrowns, and terpyridine, featuring chelates such as Cu(II) and Zn(II). Additionally, macrocyclic or iminodiacetate complexes with lanthanides like La(III), Lu(III), Eu(III) and Th(III) represent some of the cutting-edge artificial ribonucleases with metal dependency.

As discussed above, the efficiency of RNA cleavage can be enhanced through any of the following four methods: (i) facilitating deprotonation of the attacking nucleophile (2′-OH), (ii) protonating the departing group (5′-O), (iii) protonating the

non-bridging phosphoryl oxygen, and (iv) promoting the "in-line" geometry necessary for the 2´-OH to attack on the bridging phosphorus atom. aRNases leverage one or a combination of these catalytic mechanisms in a cooperative manner, depending on the specific catalytic groups involved in the process.

1.4.2   The guiding strand

The guiding strand is a complementary nucleic acid sequence that base pairs with the target RNA substrate to ensure sequence specificity. The guiding strand[63,101] aligns the ribonuclease with the target RNA, positioning the catalytic core at the precise location where cleavage is desired. Improving the reactivity of phosphodiester bonds within the target RNA through conformational alterations[102,103] has the potential to reveal specific bonds or regions, rendering them more susceptible to efficient cleavage by cleaving agents. Nevertheless, it is crucial to take into account the structural integrity and functional prerequisites of the target RNA as excessive twisting may misalign the cleavage site in relation to the cleaving agent leading to little or no hydrolysis.[102] Besides sequence, the chemical nature of the backbone such as in DNA, RNA (with sugar modifications) or peptide backbone[78,82,89,95,104,105] contributes to the overall stability and functionality of the guiding strand. RNase H can be recruited to cleave RNA in the presence of a DNA backbone.[106] Awareness of this possibility is crucial when designing artificial RNases with DNA guiding sequences. Presently, more studies have been conducted with DNA/RNA than with PNA backbone. However, peptide oligonucleotides are gaining attention due to their higher affinity and greater specificity when compared to DNA or modified RNA.

1.4.3   The linker

The linker serves as a bridge between the catalytic moiety and the guiding strand.[63] The effectiveness of site-selective RNA hydrolysis is influenced by the precise delivery of a flexible linker to the targeted cleavage site.[90] It is crucial to emphasize that the linker must be meticulously tailored, possessing the optimal length neither excessively short nor overly long, and striking the right balance between rigidity and flexibility.[90,107,108] The aminohexyl linker[63] appears to offer sufficient flexibility to catalytic groups, thereby enhancing the cleavage of phosphodiester bonds. Other examples of linkers are polyethylene glycol (PEG),[109] glyceryl,[110] diaminopropionic acid[111] and 3-(3-hydroxypropyl).[79] Altering the linker type has been observed to induce a switch in specificity.[87] An investigation into the impact of linker length and structure on ribonuclease activity revealed that a reduction in linker length [87,90,108] from two to one diethylene glycol units resulted in a significant

decrease in the conjugate's ribonuclease activity, with the maximum conversion dropping from about 12% to 3%.

1.4.4   Artificial ribozymes and DNAzymes

Ribozymes, intricate RNA molecules with catalytic abilities, are proficient in cleaving RNA substrates with precision. DNAzymes, their DNA counterparts, possess analogous cleavage capabilities.[112] The innovation of ribozymes and DNAzymes has led to their manipulation to perform an array of functions encompassing sequence-specific RNA cleavage, aptamer-mediated target recognition, and signal amplification for diagnostic applications. DNAzymes house a DNA catalytic core[113] that often relies on metal ions for its catalytic activity. The catalytic potential of DNAzymes [114] and artificial ribozymes, [115] synthetic nucleic acid molecules designed for specific chemical reactions, emerged through in vitro selection techniques, unveiling DNA sequences endowed with metal-dependent cleavage capacities. *In vitro* selection, using SELEX, begins with synthesizing a pool of random DNA sequences, exposing it to the target molecule, retaining sequences that bind, and amplifying them through PCR in multiple selection rounds. The selected DNA sequences are characterized to identify those with catalytic activity, and further optimization may be done to enhance efficiency and specificity.

2   Aims of Thesis

Recent progress in the medicinal and pharmaceutical sectors has led to growing interest in antisense technology, promising solutions to various therapeutic challenges. Antisense technology offers therapeutic potential for various diseases by selectively modulating the expression of disease-related genes. Antisense oligonucleotides rely on RNase H for mRNA target cleavage, featuring an "RNase H window" with relatively unmodified (DNA backbone) residues in the middle of their sequence.

Enhancing the efficacy of antisense oligonucleotides requires extensive modifications to improve cellular uptake and nuclease stability. However, such modifications often come at the expense of losing the ability to activate RNase H. An elegant alternative involves designing artificial ribonucleases that exhibit both catalytic efficiency and selectivity without relying on traditional RNase H functions

Among the most efficient artificial ribonucleases are those employing catalytic metal ions, typically Cu(II) or Zn(II). However, these agents, acting as coordination complexes, face challenges as they dissociate under highly diluted and metal-deficient conditions, such as those found in the intracellular medium.

This thesis aims to contribute to the field of nucleic acid hydrolysis by investigating the cleavage of phosphodiester bonds using organometallic compounds. Organometallic oligonucleotides have the potential to merge the stability of organic molecules with the catalytic effectiveness of metal complexes. Notably, the covalent carbon-metal bond in these oligonucleotides remains stable even under extreme dilution, presenting a promising solution to stability challenges encountered in metal-dependent artificial ribonucleases. Hg(II) was chosen as the catalytic metal center owing to hydrolytic stability and easy availability of arylmercury complexes. Given that the recognized toxicity of organomercury compounds stems from their tendency for lipophilic bioaccumulation, conjugation to a hydrophilic moiety, such as an oligonucleotide, is anticipated to render the cleaving agent less toxic.

3 Results and Discussions

3.1 Synthesis

3.1.1 Synthesis of RNA phosphate and thiophosphate model compounds

The choice of an adenosine-based model stems from its lower binding affinity with mercury compared to the other nucleosides. Additionally, the presence of a permanent methylene protection on the 5′-linked nucleoside simplifies the analysis of the cleavage reaction. This protection ensures that distinct sets of products are achieved from the 3′- and 5′-linked nucleosides, even in the event of potential dephosphorylation. The synthesis of adenylyl-3′,5′-(2′,3′-O-methyleneadenosine)
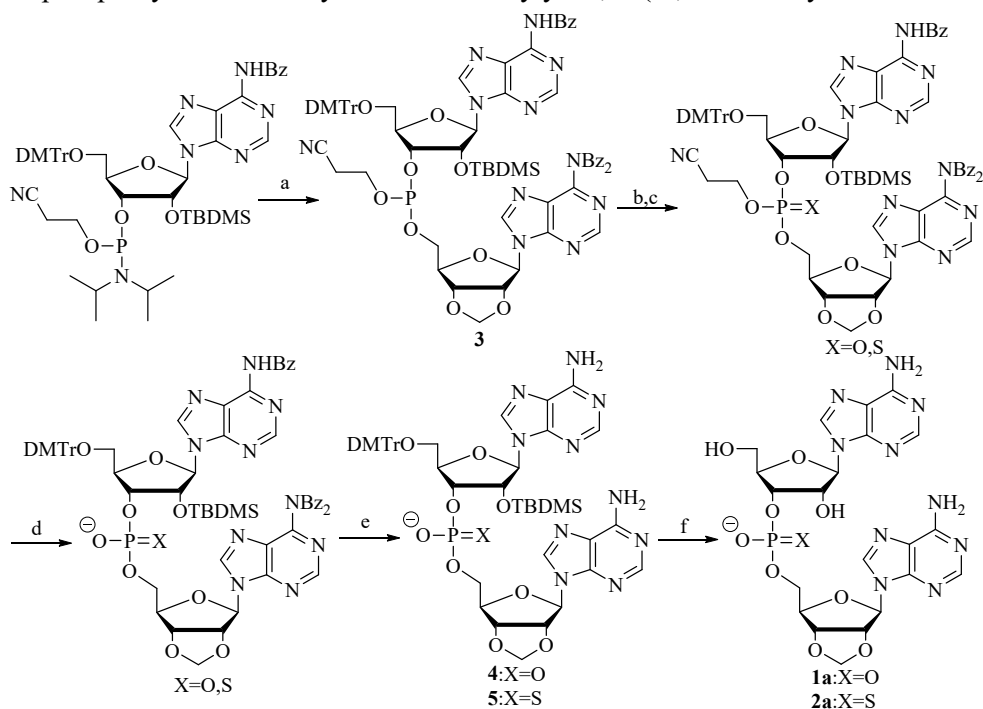
Scheme 15. Reagents and conditions: (a) 3,5-(benzylthio)-1H-tetrazole, MeCN; N$_2$ atmosphere, 25 °C, 15 min; (b) I$_2$, THF, H$_2$O, 2,6-lutidine, 25 °C, 5 min; (c) S$_8$, CH$_2$Cl$_2$, 25 °C, 16 h; (d) Et$_3$N, pyridine, 25 °C, 16 h; (e) NH$_3$, MeNH$_2$, H$_2$O, 25 °C, 1 h; (f) Et$_3$N•3HF, CH$_2$Cl$_2$, 25 °C, 72 h.

1a and adenylyl-3´,5´-(2´,3´-*O*-methyleneadenosine) phosphoromonothioate **2a** (Scheme 15) involved several steps. Commencing with utilization of 5-(benzylthio)-1*H*-tetrazole as an activator, the diisopropylamino ligand on adenosine 3´-(2-cyanoethyl-*N*,*N*-diisopropylphosphoramidite) was displaced by N^6,N^6-dibenzoyl-2´,3´-*O*-methyleneadenosine, resulting in the formation of a phosphite triester. The phosphite was then oxidized by treatment with either iodine plus water or sulfur, followed by a mixture of pyridine and triethylamine (Et₃N) to remove the cyanoethyl group. The benzoyl groups were cleaved using a mixture of aqueous ammonia and methylamine. The *tert*-butyldimethylsilyl and dimethoxytrityl groups were removed using triethylamine trihydrofluoride (Et₃N●3HF). Finally, the compounds were purified by RP–HPLC to obtain **1a** and **2a** (*S*p and *R*p diastereomers, which were differentiated based on their ³¹P NMR chemical shifts).[116]

3.1.2   Synthesis of the arylmercury cleaving agent

(2-((14-hydroxy-3,6,9,12-tetraoxatetradecyl)oxy)-3,5-dimethylphenyl)mercury (**7-Hg**), was synthesized following the procedure outlined in Scheme 16. The synthesis commenced by subjecting pentaethylene glycol to tosylation using silver oxide and sodium iodide in dichloromethane. Subsequently, the monotosylated pentaethylene glycol underwent alkylation with 2,4-dimethylphenol in the presence of potassium carbonate dissolved in dimethylformamide. Finally, the resulting compound was mercurated by treating it with mercuric acetate in CD₃OD. Purification of the product was achieved using RP-HPLC.
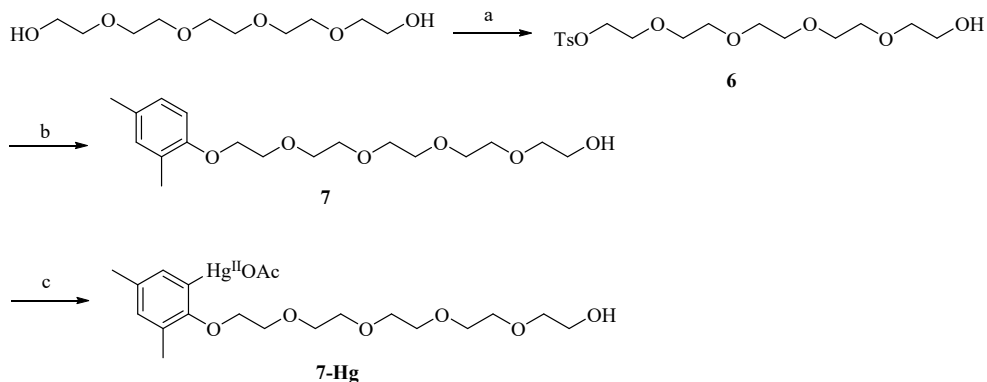
Scheme 16. Reagents and conditions: (a) Ag₂O, NaI, TsCl, dry CH₂Cl₂, 0 °C, 30 min; (b) 2,4-dimethylphenol, K₂CO₃, dry DMF, overnight; (c) Hg(OAc)₂, CD₃OD, 50 °C, overnight.

3.1.3   Synthesis of the phosphoramidite building block

The phosphoramidite building block **9** was synthesized using the method described in Scheme 17. Compound **8** was prepared in a similar manner as compound **7** in Scheme 16. Compound **8** underwent treatment with 2-cyanoethyl-*N*,*N*-diisopropylchlorophosphoramidite and triethylamine in dichloromethane.
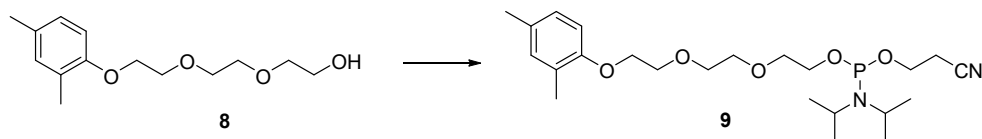
Scheme 17. Reagents and conditions: 2-cyanoethyl-*N*,*N*-diisopropylchlorophosphoramidite, Et₃N, CH₂Cl₂, N₂ atmosphere, 25 °C, 2 h.

3.1.4   Synthesis of oligonucleotide cleaving agents and their matching target strand

Table 1 presents a summary of the oligonucleotide sequences employed in this study. These oligonucleotides were synthesized using the conventional phosphoramidite method on an automated oligonucleotide synthesizer. The target strand **ON2** comprised standard commercial building blocks, with a single RNA residue placed at the specified cleavage site, while the remaining sequence was 2´-*O*-methylated. To synthesize the artificial ribonuclease oligonucleotides **ON1x-Hg** and **ON1y-Hg₂**, we utilized commercial 2´-OMe-RNA building blocks. In both cases, the building block responsible for creating a metalation site (either **8** or the previously reported 2-(phthaliminooxy)ethyl-2-cyanoethyl-*N*,*N*-diisopropylphosphoramidite[117,118]) was attached at the 5´-terminus as seen in Scheme 18. Furthermore, C5-methylated versions of cytidine and uridine building blocks were incorporated into **ON1x** to prevent mercuration of reactive sites within these nucleotides.

Table 1. The oligonucleotides sequence used in the hybridization and kinetic studies.

Oligonucleotides	Sequenceᵃ
ON1x	5´-X cᵐga cᵐcᵐg auᵐcᵐ cᵐag cᵐgg-3´
ON1x-Hg	5´-Hg-X cᵐga cᵐcᵐg auᵐcᵐ cᵐag cᵐgg -3´
ON1y	5´-Y cga ccg auc cag cgg-3´
ON1y-Hg	5´-Hg₂-Y cga ccg auc cag cgg-3´
ON2	5´-ccg cug gau cgg ucG aga gga gug a-3´

ᵃLowercase letters indicate 2´-*O*-methylribonucleotide while the capital letter G represent ribonucleotide residue. The abbreviations "cᵐ" and "uᵐ" represent C5-methylated versions of the respective nucleotides. Refer to Scheme 18 for the structures of the modified residues X, Hg-X, Y and Hg₂-Y.

For the preparation of compounds **ON1y** and **ON1y-Hg₂**, the phthaloyl protection was removed while the crude oligonucleotides were still attached on the solid support. This was accomplished by treating with a mixture of hydrazine hydrate, pyridine, and acetic acid. After the phthaloyl protection was removed, the exposed aminooxy group was promptly utilized for oxime coupling, with either 4-hydroxybenzaldehyde or 3,5-bis(acetoxymercury)-4-hydroxybenzaldehyde.[119] The specific procedure for this coupling reaction can be found in the literature[120] and is outlined in Scheme 18B. Subsequently, all oligonucleotides were released from the solid support, and the base and phosphate protections were conventionally removed through ammonolysis. In contrast to **ON1y**, **ON1x** underwent mercuration while in the solution phase using mercuric acetate (Scheme 18A). Finally, all oligonucleotides were purified using RP-HPLC, characterized through mass spectrometry, and quantified using UV spectrophotometry.
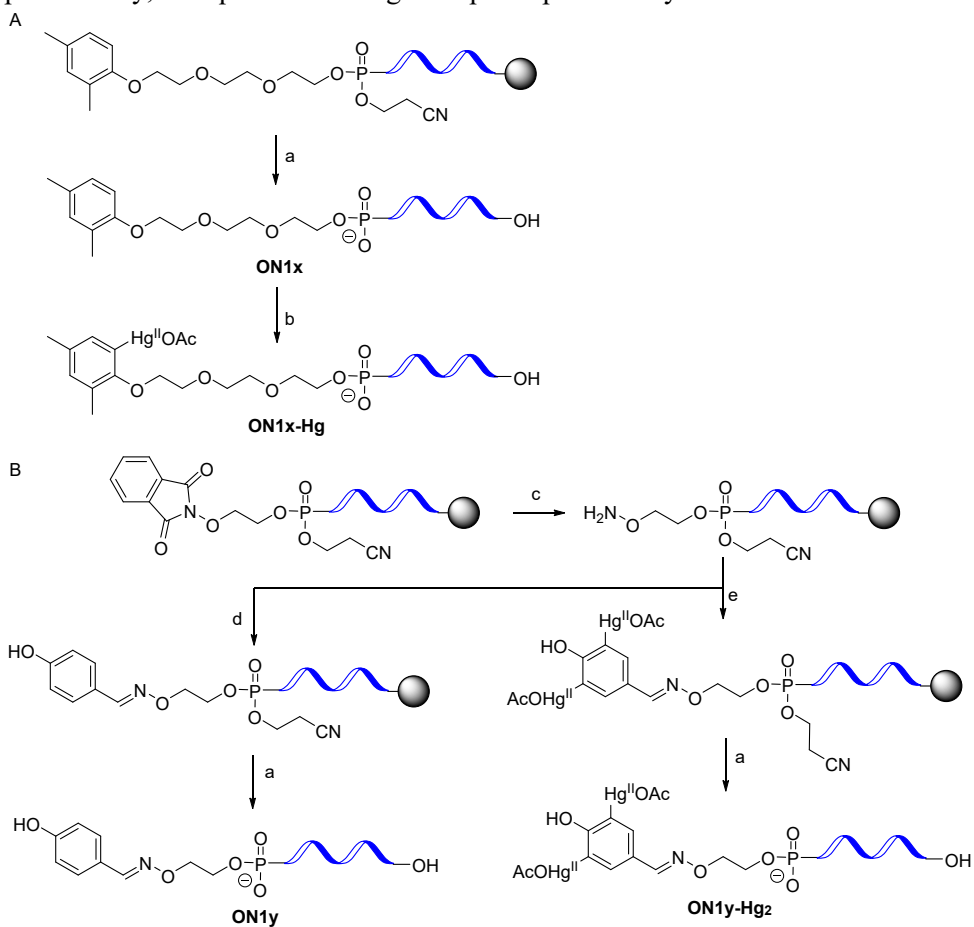
Scheme 18. Preparation of oligonucleotide conjugates A) **ON1x** and **ON1x-Hg** and B) **ON1y** and **ON1y-Hg₂**. Reagents and conditions: a) NH_3, H_2O, 25 °C, 16 h; b) $Hg(OAc)_2$, H_2O, 55 °C, 22 h; c) H_2NNH_2, H_2O, AcOH, pyridine, 25 °C, 16 h; 45 min; d) 4-hydroxybenzaldehyde, pyridine, 25 °C, 2 h; e) 3,5-bis(acetoxymercury)-4-hydroxybenzaldehyde, pyridine, 25 °C, 2 h.

3.2 Hybridization Studies

Incorporating conjugate groups into an oligonucleotide has the potential to alter its binding affinity with other molecules, as compared to the original unmodified sequence. These changes in binding strength can be assessed by studying the melting temperature (T_m).[121] The T_m represents the temperature at which half of the double helix structure of the nucleic acid unravels into single strands, as depicted in Figure 3. This process can be observed through UV spectroscopy. As the double-stranded molecule denatures, there is an increase in UV absorption, known as the hyperchromic effect. By plotting the absorbance against temperature, a sigmoidal melting curve is obtained, and the T_m value of the duplex can be determined by identifying the point of inflection on the curve.
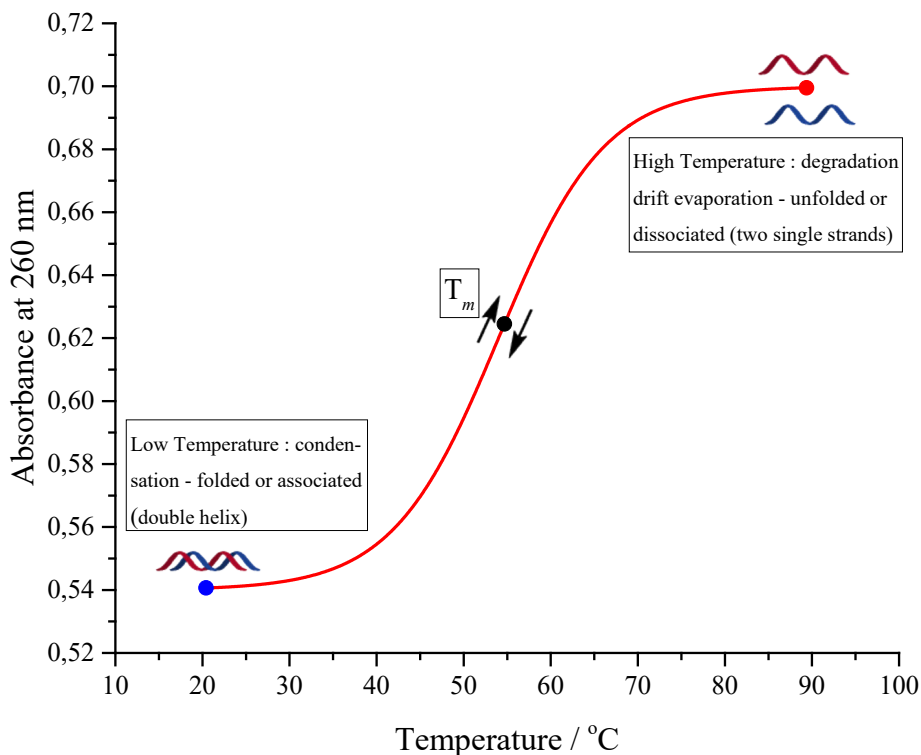
Figure 3. Nucleic acids undergo thermal denaturation, which can be detected using UV spectroscopy.

To assess the hybridization affinity of **ON1x**, **ON1x-Hg**, **ON1y**, and **ON1y-Hg$_2$**, they were each mixed with **ON2** (Scheme 19). The conjugate groups were intended to interact with the phosphodiester bond for cleavage, rather than the bases through H-bonding or metal coordination.

ON2   5´- CCG CUG GAU CGG UCG* AGA GGA GUG A - 3´

ON1R   5´- **R**CGA CCG AUC CAG CGG - 3´

hybridization

5´- CCG CUG GAU CGG UCG* AGA GGA GUG A - 3´

| | | | | | | | | | | | | | | | | |
| | | | | | | | | | | | | | | | | |

3´- GGC GAC CUA GCC AGC**R** - 5´

R: X, H-X, Y, and Hg$_2$Y

Scheme 19. Schematic representation of UV Melting experiments by mixing **ON1x**, **ON1x-Hg**, **ON1y** or **ON1y-Hg$_2$** with **ON2**. The dashes represent Watson-Crick base pairing.

A higher temperature may be necessary in the current case to achieve a reasonable reaction rate for kinetic studies (Figure 4). However, excessively high temperatures could have a negative impact on the hybridization of the aRNase with the target sequence **ON2**. To determine the highest temperature that can be applied,

Figure 4. UV melting profile of duplexes of **A) ON1x•ON2, B) ON1x-Hg•ON2, C) ON1y•ON2 and D) ON1y-Hg$_2$•ON2**; [oligonucleotides] = 1.0 μM; pH = 7.4 (20 mM cacodylate buffer); I(NaClO$_4$) = 0.10 M.

UV melting profiles were recorded for the duplexes formed by **ON1x**, **ON1x-Hg**, **ON1y**, and **ON1y-Hg$_2$** with the target oligonucleotide **ON2**. These profiles were recorded over a temperature range of 10—90 °C at pH 7.4 (using a 20 mM cacodylate buffer) and an ionic strength of 0.10 M (adjusted with sodium perchlorate). The melting temperatures of all duplexes were too high to be accurately determined, and no denaturation was observed below 60 °C. Therefore, a temperature of 55 °C was chosen as suitable for the kinetic studies.

3.3 Kinetics of Hg(II)- and arylmercury complexes-catalyzed cleavage and isomerization of adenylyl-3′,5′-(2′,3′-*O*-methyleneadenosine)

The cleavage of the phosphodiester bond in the RNA model compound **1a** was observed at 90 °C. This process was monitored through RP–HPLC while maintaining an ionic strength of 0.10 M, adjusted by sodium nitrate. Reactions catalyzed by Hg(II) were conducted over a pH range of 5.0–6.0 using a 30 mM MES buffer. On the other hand, arylmercury (**7-Hg**)–catalyzed experiments covered a broader pH range of 3.0–8.5, employing various buffers such as formic, MES, HEPES, and glycine. Compared to Hg(II), **7-Hg** has improved water solubility, thanks to its hydrophilic pentaethylene glycol tail, which expanded the pH range investigated. This distinction was evident in the clear appearance of the reaction solutions. Before conducting the analysis, sodium chloride was introduced to the samples to precipitate Hg(II) in the form of the tetrachlorido complex. Irrespective of the presence of these catalysts, **1a** underwent partial conversion to its 2′,5′-isomer
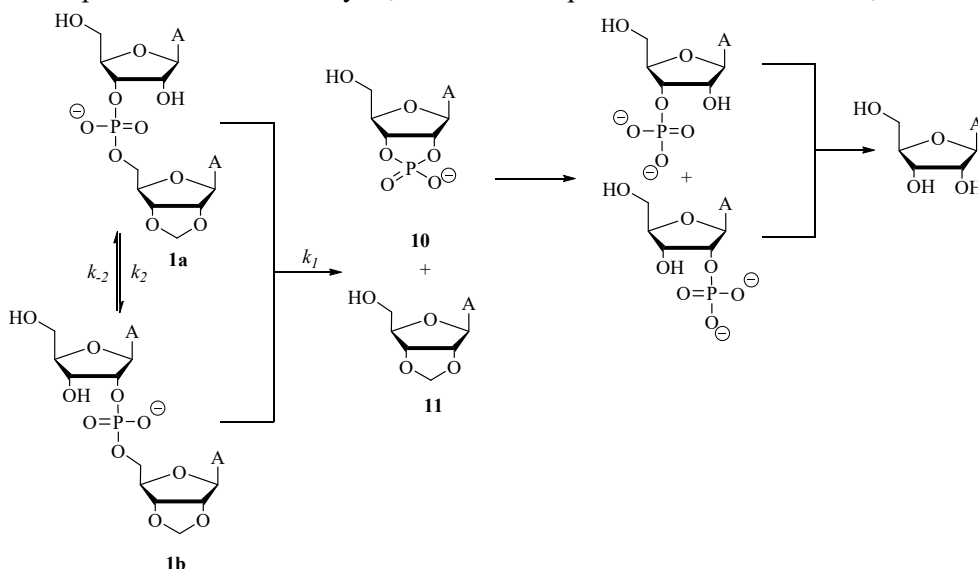
Scheme 20. Hydrolytic reaction pathways of **1a** and its 2′–isomer **1b**.

1b (Scheme 20). The resulting isomeric mixtures were then cleaved into **11** and **10**. Subsequently, **10** underwent hydrolysis to yield adenosine without accumulation of the 2´/3´-AMP intermediate. The rates of these final two reactions were too slow to be reliably quantified.

To assess the influence of [Hg(II)] on the cleavage and isomerization rates of **1a** a thorough examination was conducted across a concentration range of 0–5 mM at pH 6.0 utilizing a 30 mM MES buffer (Figure 5). Both sets of reactions displayed a consistent rate pattern dependent on [Hg(II)] at low concentration, with a plateau at higher concentrations. The presence of 5 mM Hg(II) significantly influenced the reaction rate, by 20-fold when compared to the reaction in the absence of Hg(II). Previously, similar acceleration had been observed in the case of other divalent transition metal ions, including Zn(II).[58]

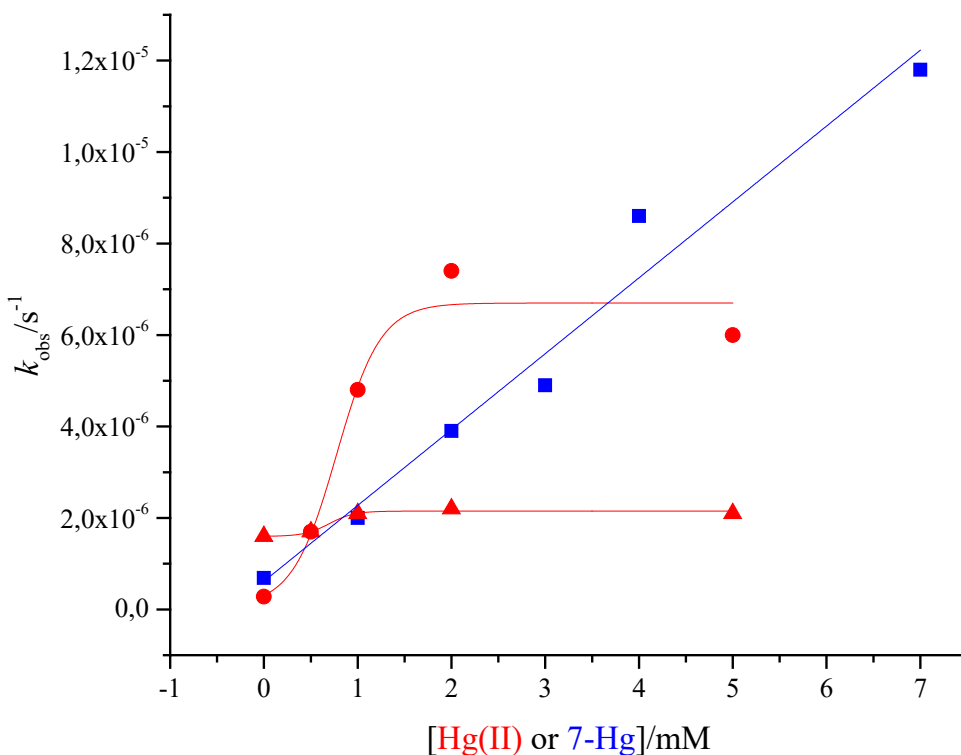**Figure 5.** **[Hg(II)]**- and **[7-Hg]**-dependence for the cleavage of **1a** are represented by red cycle and blue square respectively, while the red triangle represent isomerization in the presence of **Hg(II).** T = 90 °C; pH = 6.0; [buffer] = 30 mM; I(NaNO$_3$) = 100 mM.

Equation (1) captures the correlation between the observed pseudo first-order rate constant and the concentration of Hg(II) in both instances.

$$k^{obs} = k^0 + \frac{k^{Hg}[\mathbf{H_g}]^n}{K_d n + [\mathbf{H_g}]^n} \tag{1}$$

The rate constants for reactions involving Hg(II), both in the absence (k^0) and presence (k^{Hg}) of Hg(II) catalysis, are designated as first- and nth-order, respectively. The dissociation constant of the reactive complex is denoted as K_d, and the reaction order with respect to the Hg(II) ion is represented by n. The uncertainty of this value is considerable; however, the sigmoidal plots derived from both reactions strongly suggest the involvement of multiple Hg(II) ions. The values of these rate constants, obtained through non-linear least-squares fitting of experimental data to Equation (1), are consolidated in Table 2.

Table 2. Presents the kinetic parameters for the Hg(II)-catalyzed cleavage (k_1) and isomerization ($k_2 + k_{-2}$) reactions of **1a** and **1b** under the following conditions: T = 90 °C, pH = 6.0, buffer concentration of 30 mM, and I(NaNO$_3$) = 100 mM.

	$k^0/10^{-7}$ s^{-1}	$k^{Hg}/10^{-6}$ M^{-n} s^{-1}	n
k_1	2.8 ± 0.1	7 ± 2	3 ± 10
$k_2 + k_{-2}$	14 ± 1	1.3 ± 0.2	3 ± 6

The dissociation constants for the reactive complex were similar for both the cleavage and isomerization reactions (K_d = 0.8 and 0.63 mM, respectively), resembling those observed for the Hg(II)–adenosine complex.[122] Previous studies[123–125] have shown that adenosine 5′-monophosphate exhibits a capacity for the formation of indirect chelates with divalent transition metal ions. In this context, an aqua ligand associated with an N7–coordinated metal ion forms a hydrogen bond with the phosphate moiety. This proposed binding mode aligns with the observed catalytic activity, which would suggest its relevance in the current scenario.

The impact of [**7-Hg**] on the rate of cleavage of **1a** and **1b** was investigated at pH 7.0, utilizing a 30 mM HEPES buffer. Across the concentration range of 0–7 mM, the reaction rate exhibited a linear dependence on the concentration of **7-Hg**, resulting in 3–17-fold accelerations (Figure 5). As the concentration of **7-Hg** surpassed 7 mM, the reaction solution exhibited turbidity, indicative of the likely precipitation of **7-Hg**. The linear [**7-Hg**]–dependence suggests that the association constant between **1a** (or **1b**) and **7-Hg**, governing the formation of the reactive complex, is too low to determine accurately due to the limited solubility of **7-Hg**. Consistent with this finding, previous observations[122] have indicated that the association constant of MeHg(II) with both adenine ring nitrogens and oxygen donors is over an order of magnitude lower than that of Hg(II). The apparent second-order rate constant for the (**7-Hg**)–catalyzed reaction, denoted as k_1^{cat} and derived from the slope of the linear plot, was determined to be $(1.7 \pm 2) \times 10^{-3}$ M^{-1} s^{-1}.

Concentration–dependence studies on Hg(II) and **7-Hg** play a crucial role in establishing the optimal catalyst concentration for other kinetic studies. In the absence of a catalyst, the pH–rate profile for the cleavage of compounds **1a** and **1b** (Figure 6) exhibited a reaction catalyzed by hydronium ions (first order in $[H^+]$) at pH values below 5.0, a pH-independent reaction from pH 5 to 6, and a reaction catalyzed by hydroxide ions (first order in $[OH^-]$) at pH values greater than 6, which aligns with findings from previous studies on similar systems.[37,43] The catalysis facilitated by 1 mM **7-Hg** reveals intriguing distinctions within the pH range of 5.0 to 7.0. Notably, within the pH range of 6.0 to 7.0, the cleavage reaction catalyzed by **7-Hg** exhibited an additional plateau, and at pH 5.0–6.0, a second–order dependence on $[OH^-]$. The presence of **7-Hg** did not have a significant impact on the rate of mutual isomerization between compounds **1a** and **1b**. Across the whole pH range examined, the process of breaking the bond happened notably faster compared to that of isomerization in the presence of a catalyst. At a saturating concentration of Hg(II) (5 mM), the reaction appeared to slow first-order dependence on hydronium
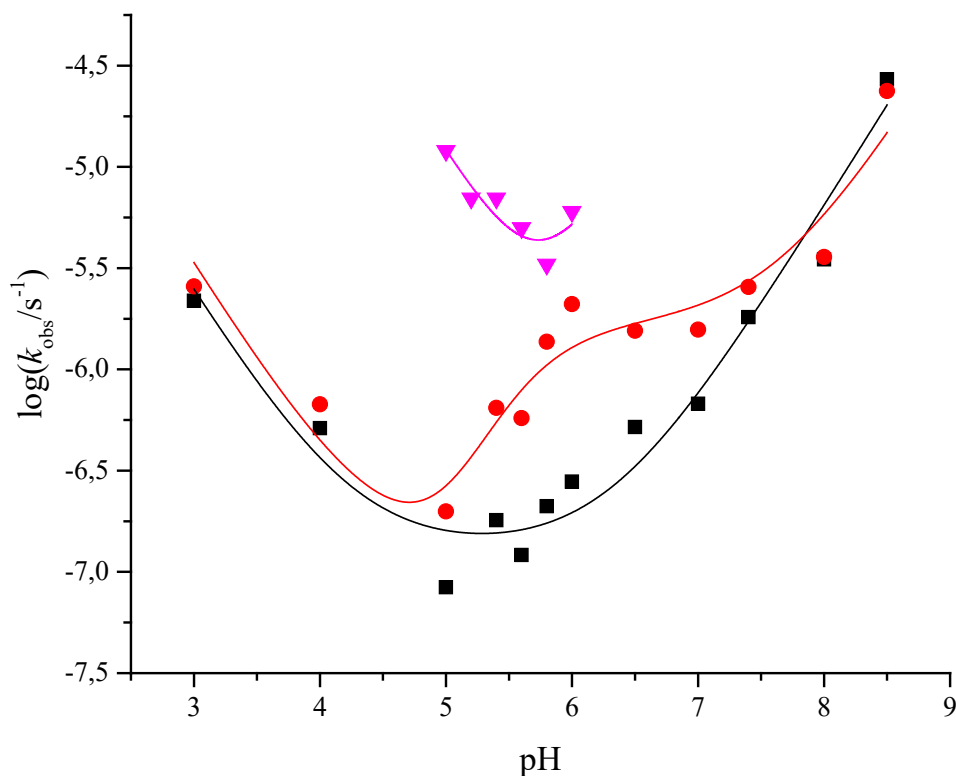

Figure 6. pH-rate profiles for the cleavage of **1a** in the presence of **Hg(II)** represented by the filled magenta triangle, in the presence of **7-Hg** represented by filled red circle and in the absence of any catalyst is represented by filled black squares; T = 90 °C; [Hg(II)] = 5 mM; [**7-Hg**] = 1 mM; [buffer] = 30 mM; I(NaNO$_3$) = 100 mM.

ion between pH 5.0 to 5.6. However, as the pH approached 6.0, a shift to first-order dependence on hydroxide ion took place. The hydronium and hydroxide ion catalyzed reactions were both orders of magnitude faster than the respective reactions in the absence of a metal catalyst.

Table 3. Kinetic parameters for Hg(II) and [**7-Hg**]-catalyzed cleavage (k_1) of **1a** and **1b**; $T = 90$ °C; [buffer] = 30 mM; I(NaNO$_3$) = 100 mM.

|	no catalyst	5.0 mM Hg(II)	1.0 mM 7-Hg
k_1^H / 10^{-3} M^{-1} s^{-1}	2.4 ± 0.9	1200 ± 200	3.2 ± 1.4
$k_1^{H_2O}$ / 1^{-7} s^{-1}	1.3 ± 0.3	n.a.	1.2 ± 1.6
k_1^{OH} / M^{-1} s^{-1}	0.10 ± 0.02	6.5 ± 1.5	0.07 ± 0.03
k_1^{cat} / 10^{-3} M^{-1} s^{-1}	n.a	n.a	1.6 ± 0.5
$K_{a1} = K_{a2}$ / 10^{-6} M	n.a	n.a	3 ± 2

Table 3 summarizes the rate and equilibrium constants obtained through non-linear least squares fitting of the experimental data to Equation (2), which accounts for both pH-independent reactions, hydronium ion and hydroxide ion catalyzed reactions, providing a comprehensive understanding of the system's kinetics which can also be seen in figure 6. In these studies, k_1^{obs} represents the observed rate constant. $k_1^{H_2O}$ represents the first-order rate constant for pH-independent cleavage, k_1^H, k_1^{OH} and k_1^{cat}

$$k_1^{obs} = k_1^H[\mathbf{H^+}] + k_1^{H_2O} + \frac{k_1^{cat}[\mathbf{7-H_g}]K_{a_1}K_{a_2}}{[\mathbf{H^+}]^2 + K_{a_1}[\mathbf{H^+}] + K_{a_1}K_{a_2}} + \frac{k_1^{OH}K_W}{[\mathbf{H^+}]} \tag{2}$$

denote the second-rate constants[43] associated with the hydronium ion, hydroxide ion and (**7-Hg**)-catalyzed cleavage, respectively, and K_W (6.2×10^{-13} M^2) represents the ion product of the water under the experimental conditions. The significance of the kinetic acid dissociation constants, K_{a1} and K_{a2}, is not fully understood. However, these constants are needed for proper fitting of the second order dependence on [OH$^-$] between pH 5 and 6 and the plateau between pH 6 and 7 in Figure 6 and they are likely associated with protolytic equilibria that involve an Hg(II) aqua ligand and/or an adenine base.[37] The observed second-order dependence on [OH$^-$] between pH 5 and 6 indicates that these two constants must have very close values, rendering them practically indistinguishable from each other.

The modest acceleration of the isomerization of compounds **1a** and **1b** exhibits a similarity to previous findings on the catalytic effects of various metal ions.[37] This suggests that the breakdown of **1a** and **1b** is due to assistance in departure of the 5′-linked nucleoside, which occurs either through direct coordination of Hg(II) with the 5′-oxygen or by the transfer of a proton from an aqua ligand. Although both scenarios are possible, the latter seems more plausible as it offers a reasonable explanation for

one of the observed acid dissociation constants. In this proposed mechanism, a proton is transferred from the attacking 2′-oxygen to an Hg(II) hydroxo ligand in a rapid pre-equilibrium step (Scheme 21), followed by a transfer from an Hg(II) aqua ligand to the departing 5′-O. This transfer process, along with the rate–limiting breaking of the P–O bond, accounts for the overall cleavage of **1a** and **1b**. Notably, a similar mechanism has been previously suggested for the cleavage of a model compound guanylyl-(3′,3′)–(2′-amino-2′-deoxyuridine), which possesses an unprotonated amino group adjacent to the departing 3′-oxygen.[126] The presence of another observed acid dissociation constant likely corresponds to the formation of a reactive complex, potentially through interaction with the adenine base of the departing nucleoside. The exact nature of this interaction remains unclear, but the simultaneous loss of a proton suggests possible coordination with the exocyclic amino group.[127,128]
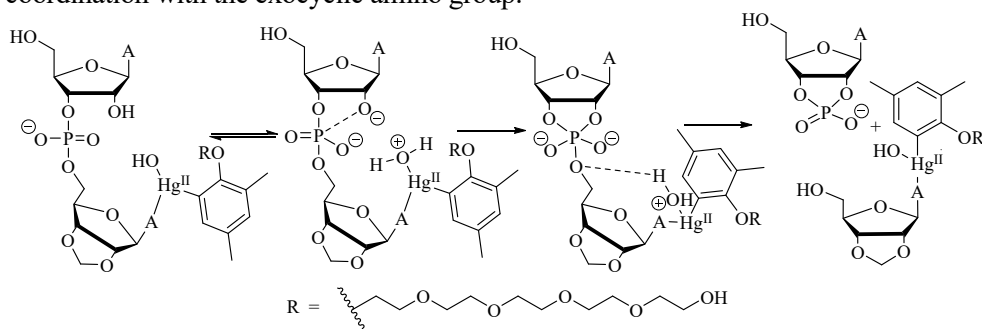
Scheme 21. Proposed mechanism for the cleavage of **1a** catalyzed by **7-Hg**.

3.4 Kinetics of Hg(II)-catalyzed desulfurization of adenylyl-3′,5′-(2′,3′-*O*-methyleneadenosine) phosphoromonothioate

The rates of desulfurization of R_p and S_p diastereomers of phosphoromonothioate **2a** were examined separately at pH 6.9 and 0 °C. The analysis was carried out without and with 20 μM of Hg(II). Sodium nitrate was included to maintain an ionic strength of 0.10 M. When **2a** underwent desulfurization (k_4 in Scheme 22), it yielded a mixture of two isomeric products: **1a** and **1b** and two cleaved products: **10** and **11.**
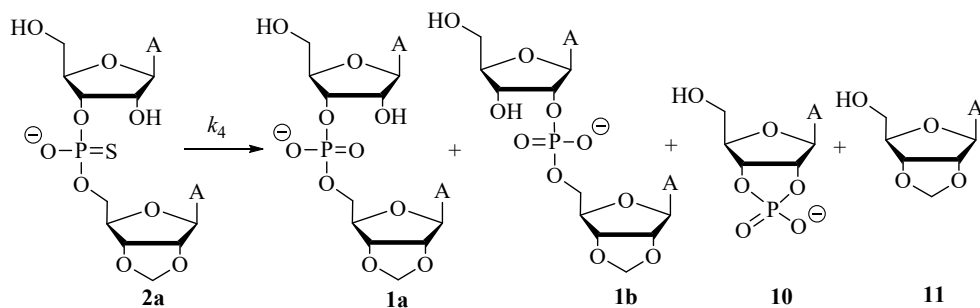

Scheme 22. Desulfurization of **2a** resulting in both isomerization and cleaved products.

The observed product ratio was 5:4:1:1. According to previous literature,[129] the desulfurization process of ribonucleoside phosphoromonothioates initiates with a nucleophilic attack by the neighboring OH group, forming an intermediate with five coordinated atoms. Subsequent removal of hydrogen sulfide (or mercuric sulfide in the presence of Hg(II)) from this intermediate creates a cyclic phosphotriester. The cyclic phosphotriester then quickly decomposes by breaking either one of the internal P–O bonds, resulting in the formation of **1a** or **1b**, or the external P–O bond, leading to the formation of **10** and **11**. This mechanism also explains the previously reported competition between cleavage and desulfurization.[130] Desulfurization consistently occurs first, and the competition involves the breaking of the internal and external P–O bonds. In the absence of Hg(II), the desulfurization rates for both diastereomers of **2a** were nearly identical ($k_4 = 7 \pm 2$ and $6 \pm 2 \times 10^{-8}$ s^{-1} for S_p and R_p diastereomers, respectively). The presence of Hg(II) did not impact the product distribution, but it accelerated the rate of desulfurization by more than four orders of magnitude ($k_4 = 4 \pm 1$ and $1.4 \pm 0.1 \times 10^{-3}$ s^{-1} for S_p and R_p diastereomers, respectively).

3.5 Kinetics of Hg(II)-catalyzed depurination of 2′-deoxyadenosine

Regardless of the presence of Hg(II), depurination of 2′-deoxyadenosine was observed under the same conditions used for the hydrolytic reactions of **1a** and **1b**. Over the tested pH range, the only reaction observed was the conversion of 2′-deoxyadenosine to adenine and nonchromophoric products (k_3 in Scheme 23). The rate of this reaction was found to be dependent on the concentration of hydronium ions, exhibiting first-order kinetics both in the absence and presence (5 mM) of Hg(II) (Figure 7). The second-order rate constants were determined as $k_3^H = 1.16 \pm 0.06$ and 2.2 ± 0.2 M^{-1} s^{-1}, respectively. Previous studies[131] have reported a similar, moderate, increase in the reaction rate of 9-(1-ethoxyethyl)purine in the presence of Hg(II). This acceleration was attributed to the combined effects of electron withdrawal resulting from simultaneous protonation at N1 and coordination of Hg(II) at N7. Depurination of the ribonucleoside-based model compounds **1a** and **1b** would be much slower, probably negligible under the conditions used to study the hydrolytic reactions.
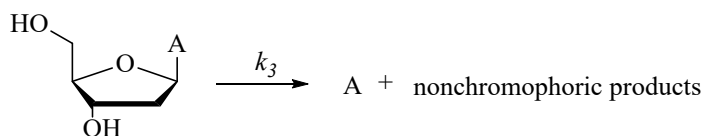
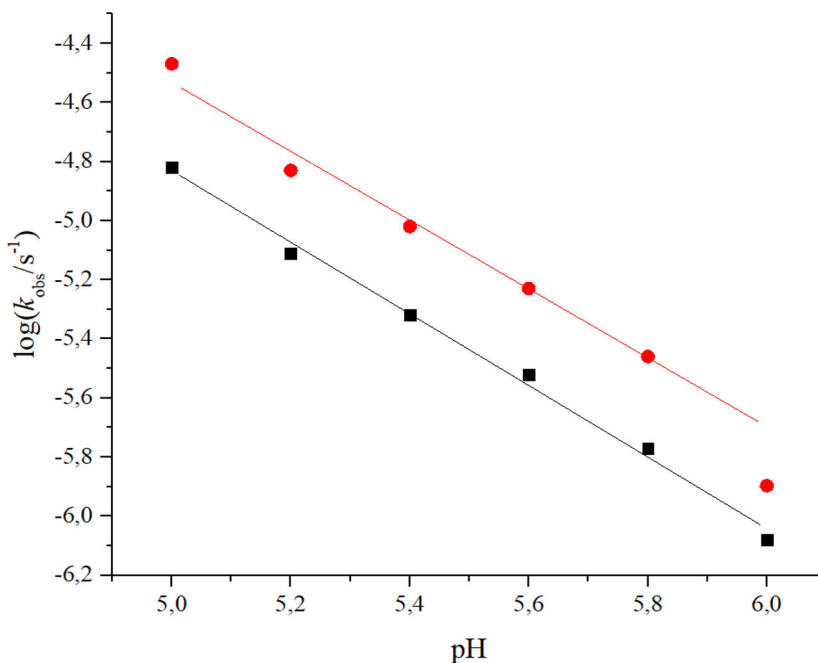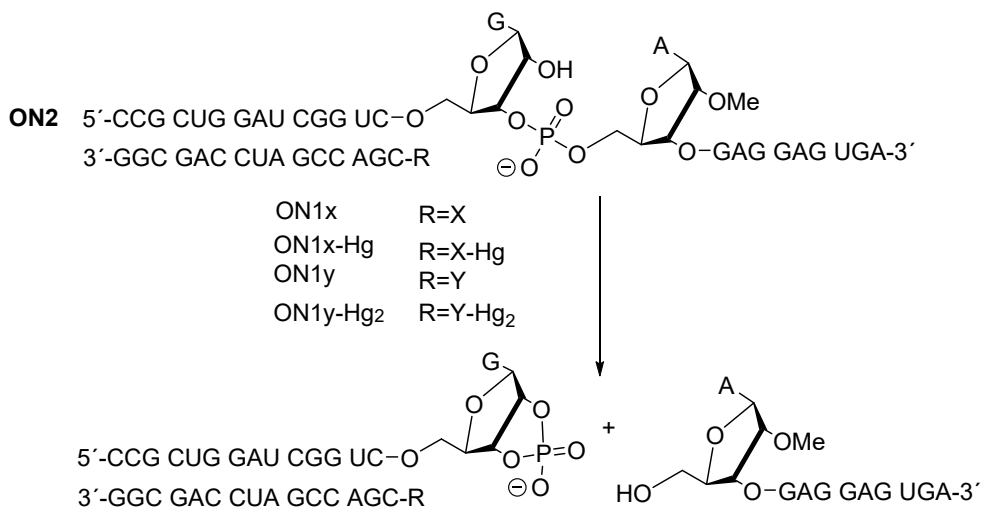**Scheme 23.** Depurination of 2′-deoxyadenosine.

Figure 7. The pH–rate profiles for the depurination (k_3) of 2′-deoxyadenosine in the absence (■) and presence (●) of Hg(II); T = 90 °C; [Hg(II)] = 0/5 mM; [buffer] = 30 mM; I(NaNO$_3$) = 100 mM.

3.6 Reaction kinetics of target strand cleavage by organomercury oligonucleotide conjugates

The objective of the study was to investigate the catalytic properties of organomercury oligonucleotide conjugates, namely **ON1x-Hg** and **ON1y-Hg₂**, in the cleavage of the complementary target oligonucleotide **ON2**. The experiments were conducted at pH 7.4, utilizing a 20 mM cacodylate buffer, and at 55 °C. **ON2** was designed with a single ribonucleotide residue at position 15, which served as the active site for cleavage, while the remaining sequence was 2′-*O*-methylated. Additionally, unmercurated cleaving agents (**ON1x** and **ON1y**) were used as control samples. At predetermined time intervals, samples were withdrawn from the reaction mixtures and subjected to analysis using anion exchange HPLC. The identification of peaks was accomplished through RP–UPLC–MS.

The two mercurated oligonucleotides **ON1x-Hg** and **ON1y-Hg₂**, functioning as artificial ribonucleases, effectively cleaved **ON2** into the anticipated products. These products consisted of a 15-mer oligonucleotide with a 2′,3′-cyclic monophosphate terminus and a 10-mer oligonucleotide with a 5′-alcohol terminus, as shown in Scheme 24. Despite extensive testing of various solvent systems, quantifying these products posed challenges due to the insufficient chromatographic separation

ON2 5´-CCG CUG GAU CGG UC–O
3´-GGC GAC CUA GCC AGC-R

ON1x	R=X
ON1x-Hg	R=X-Hg
ON1y	R=Y
ON1y-Hg2	R=Y-Hg$_2$

5´-CCG CUG GAU CGG UC–O
3´-GGC GAC CUA GCC AGC-R

Scheme 24. Cleavage of the target oligonucleotide **ON2**, catalyzed by the artificial ribonucleases **ON1x-Hg** and **ON1y-Hg$_2$**.

achieved. However, the peak corresponding to the starting material **ON2** could be consistently measured, enabling the determination of reaction rates based on its time-dependent decrease, as illustrated in Figure 8. Figure 8 illustrates the impact of different oligonucleotides on the cleavage of **ON2**. When the unmercurated
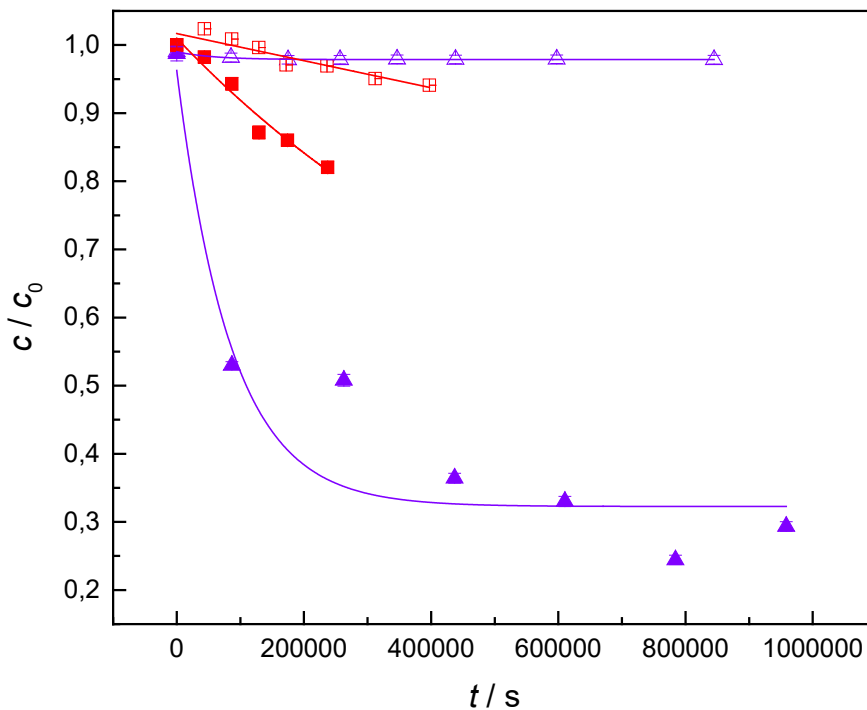

Figure 8. Time-dependent concentration of oligonucleotide **ON2** in the presence of complementary oligonucleotides **ON1x** (△), **ON1x-Hg** (▲), **ON1y** (□), **ON1y-Hg$_2$** (■); T = 55 °C; pH = 7.4 (20 mM cacodylate buffer); I(NaClO$_4$) = 0.10 M.

oligonucleotide **ON1x** was present, minimal cleavage of **ON2** was observed. However, the presence of the other unmercurated oligonucleotide **ON1y** resulted in some cleavage. In contrast, the mercurated artificial ribonucleases, **ON1x-Hg** and **ON1y-Hg₂**, exhibited significantly enhanced performances compared to their unmercurated counterparts. Among the two, **ON1x-Hg** demonstrated greater efficiency. Although a certain portion of **ON2** appeared unchanged in both cases, it is important to note that this is likely due to the overlapping peaks of **ON2** and the artificial ribonuclease, rather than a decrease in the reaction rate. Additionally, the UPLC-MS analysis revealed that both **ON1x-Hg** and **ON1y-Hg₂** remained predominantly intact at the conclusion of the kinetic runs. To determine the first-order rate constants for **ON2** cleavage, the experimental data from Figure 8 were subjected to non-linear least-squares regression, utilizing Equation 3.

$$c_t = (c_0 - c_{eq})(1 - e^{-k_{obs}t}) + c_{eq} \tag{3}$$

The relative concentrations of **ON2** at different time points are denoted as c_t, c_0 and c_{eq} at time point t, at the beginning of the kinetic run, and at equilibrium, respectively. The first-order rate constant is denoted as k_{obs}, and the sampling time is represented by t. The details of the fitting results can be found in Table 4.

Table 4. Kinetic parameters for the cleavage of the target oligonucleotide **ON2** in the presence of its complementary oligonucleotides **ON1x**, **ON1x-Hg**, **ON1y** and **ON1y-Hg₂**; T = 55 °C; pH = 7.4 (20 mM cacodylate buffer); I(NaClO₄) = 0.10 M.

	k_{obs} / 10^{-6} s^{-1}	c_0	c_{eq}
ON1x	n.a.[#]	n.a.[#]	n.a.[#]
ON1x-Hg	12 ± 4	1.0 ± 0.1	0.32 ± 0.04
ON1y	n.a.[#]	n.a.[#]	n.a.[#]
ON1y-Hg₂	2 ± 3	1.01 ± 0.02	0.4 ± 0.9

[#] Could not be established reliably due to inadequate progress of the reaction.

A comparison of the rate constants for cleavage by **ON1x-Hg** and by the respective small molecule cleaving agent **7–Hg** reveals a distinct disparity. Interestingly, the rate constant for the **ON1x-Hg**-catalyzed reaction is ten times higher than that of the **7–Hg**-catalyzed reaction, even though the latter was carried out at a higher temperature. This discrepancy highlights a significant proximity effect, wherein the presence of the **ON1x-Hg** complex close to the target phosphodiester bond enhances the reaction rate. By tethering the arylmercury complex to a complementary oligonucleotide, the local concentration of the complex near the cleavage site was increased as anticipated. The structural similarities

between the catalytic components suggest that the mechanism proposed for **7–Hg** is likely applicable also to the present scenario.

The additional Hg(II) ion in **ON1y-Hg$_2$** does not confer any catalytic advantage, indicating its unfavorable positioning for the reaction to occur. In fact, the observed rate constant for **ON1y-Hg$_2$** is significantly lower than that of **ON1x-Hg**. This disparity can be attributed to the shorter and more rigid linker in **ON1y-Hg$_2$**, which hampers the optimal interaction between the catalytic moiety and the target phosphodiester bond.

4 Conclusions

Hg(II) accelerates isomerization of adenylyl-3´,5´-(2´,3´-*O*-methyleneadenosine) by twofold and cleavage of the phosphodiester linkage by two orders of magnitude, similarly to many other divalent transition metal ions. The modest acceleration of isomerization can be attributed to electrophilic catalysis by Hg(II) ions coordinated to the scissile phosphate, and/or general base catalysis by a Hg(II) hydroxo ligand. However, the significantly more pronounced acceleration of cleavage implies the involvement of additional general acid catalysis, likely by a Hg(II) aqua ligand. The discoveries presented here position Hg(II) as a compelling and novel inclusion in the array of metal ions applicable to the development of artificial nucleases.

The potential of organomercury compounds as RNA cleaving agents was demonstrated by a 17-fold acceleration in the cleavage of adenylyl-3´,5´-(2´,3´-*O*-methyleneadenosine). While this cleaving agent demonstrates a slightly lower acceleration rate compared to Hg(II) owing to its reduced affinity for the target compound, this challenge can be effectively addressed by incorporating specific targeting groups, such as a 2´-OMe-RNA oligonucleotide. In an effort to test this approach, two organomercury oligonucleotide conjugates serving as artificial ribonucleases were synthesized. These conjugates demonstrated enhanced catalytic efficiency in comparison to their non-mercurated counterparts. Although the current performance was lower when compared with some other artificial ribonucleases, the sensitivity to linker length and rigidity suggests that significant improvement can be achieved through structural optimization. Furthermore, organometallic catalytic groups, particularly those incorporating Hg(II) or Pd(II), are expected to demonstrate robust hydrolytic stability under physiological conditions.

5 Experimental

5.1 General methods

All solvents utilized in the synthesis and purification of compounds were of reagent-grade quality. For experiments sensitive to air and/or moisture, solvents were subjected to drying using 3 or 4 Å molecular sieves. The progress of all reactions was monitored through thin-layer chromatography (TLC), conducted on Merck 60 (silica gel F254) plates, which were subsequently visualized under ultraviolet light and in some cases stained with $KMnO_4$ solution. Detailed descriptions of compound synthesis and characterization can be found in the original publications. The synthesized compounds underwent purification via silica gel (230–400 mesh) column chromatography and, when necessary, reversed phase–high performance liquid chromatography (RP-HPLC). The identities of the compounds were confirmed through various analytical techniques, including ion exchange HPLC (IE-HPLC), liquid chromatography–mass spectrometry (LC-MS), electrospray ionization mass spectrometry using Bruker micrOTOF–Q and Waters Acquity RDa spectrometers, as well as ^{1}H, ^{13}C, ^{31}P, and various 2D NMR analyses using Bruker Biospin 500 MHz NMR spectrometers. The chemical shifts are reported in parts per million (ppm), referenced to the residual solvent peak as an internal standard.

5.2 Oligonucleotide synthesis

The oligonucleotides were prepared in 1–2 µmol scale using an ÄKTA Oligopilot Plus 10 automated oligonucleotide synthesizer. Commercially available phosphoramidite building blocks were utilized and a standard phosphoramidite coupling procedure was employed to synthesize the oligonucleotides. All reactions were conducted on CPG solid supports.

When applicable, the phthaloyl protection was removed while the crude oligonucleotides were still attached on the solid support. This was accomplished by treating with a mixture of hydrazine hydrate, pyridine, and acetic acid. After the phthaloyl protection was removed, the exposed aminooxy group was promptly utilized for oxime coupling, with either 4-hydroxybenzaldehyde or 3,5-bis(acetoxymercury)-4-hydroxybenzaldehyde.[119] Finally, all oligonucleotides were

released from the solid support and protecting groups on the base and phosphate moieties were removed by incubation in 25 % aqueous ammonia at 25 ºC for overnight. The one 2′-OTBDMS protection of **ON2** was removed through treatment with a mixture of DMSO (100 μL) and triethylamine trihydrofluoride (125 μL) at 65 °C for 150 min. The solution was then cooled to −20 °C and 3 M aqueous sodium acetate (25 μL) was added. After vigorous shaking for 30 s, *n*-butanol (1.0 mL) was added, and shaking resumed for an additional 30 s. The mixture was maintained at −20 °C for 60 min, followed by centrifugation. The supernatant was decanted, and the resulting precipitate underwent washing with ethanol (2 × 750 μL). The resultant crude **ON2** was then dissolved in water. Purification of the oligonucleotides was achieved through RP-HPLC using a semi-preparative SunFire C18 column (250 × 10 mm, 5 μm). A gradient elution method was employed, transitioning from 5% to 30% acetonitrile in a 0.05 mol L^{-1} aqueous triethylammonium acetate solution over a span of 25 to 30 min, with a flow rate of 3.0 mL min^{-1} and UV detection at 260 nm. The identity and purity of the purified oligonucleotides were confirmed using a Waters Acquity RDa mass spectrometer.

5.3   Kinetic measurements

The hydrolytic reactions of the phosphodiester bond in adenylyl-3′,5′-(2′,3′-*O*-methyleneadenosine) were carried out in the absence and presence of the catalysts (Hg(II) or **7-Hg**) in sealed tubes immersed in a water bath, the temperature of which was kept at 90 °C (± 0.1 °C). The pH of the reaction solutions was adjusted with 0.030 M sodium formate, 2-(*N*-morpholino)ethanesulfonic acid (MES), *N*-(2-hydroxyethyl)piperazine-*N*′-2-ethanesulfonic acid (HEPES) and glycine buffers and the ionic strength ($I = 0.10$ M) with NaNO$_3$. Before starting to follow the reactions in the presence of catalysts, the pH of the reaction solutions was adjusted exactly to the value measured for the respective reaction solutions in the absence of catalysts by titrating with either 1.00 M NaOH or 0.88 M HNO$_3$.

Samples were withdrawn from the reaction solutions at appropriate time intervals and cooled to 0 °C to quench the hydrolysis. Compositions of the samples were determined by RP-HPLC on a Thermo Scientific Aquasil column (4 × 150 mm, 5 μm) eluting with a linear gradient of acetonitrtile (3—15% over 30 or 40 min) in 50 mM aqueous ammonium acetate. The flow rate was 1.0 mL min^{-1} and the detection wavelength 260 nm. The products were identified by spiking with authentic samples as well as by HPLC/MS analysis.

The hydrolytic reactions of the oligonucleotide substrate **ON2** were carried out in sealed tubes thermostated at 55.0 °C (± 0.1 °C). The concentration of both the target oligonucleotide and the artificial ribonuclease was set at 0.20 μM. pH adjustment to 7.4 was achieved using a 20 mM cacodylate buffer, while the ionic

strength was maintained at 0.10 M with sodium perchlorate. The samples obtained from the reaction solutions at specified time intervals were promptly cooled in an ice/water bath. To effectively halt the reactions, an excess (20 equivalents) of 2-mercaptoethanol was introduced. The sample composition was analyzed using IE-HPLC on a Thermo Scientific DNASwift SAX-1S column (150 × 5 mm, monolithic). Typically, a linear gradient (10—45% over 20 min) of 0.33 M sodium perchlorate in a 20 mM aqueous triethanolamine buffer (pH = 7.0) was employed, except in the case of the **ON1-Hg** and **ON2** reaction mixture, where a more denaturing solvent system was necessary. For the latter, a linear gradient (15—55% over 15 min) of 0.33 M sodium perchlorate in a 20 mM aqueous triethylamine buffer (pH = 10.0) was utilized. The flow rate was maintained at 1.5 mL min^{-1}, and the detection wavelength was set at 260 nm for all analyses. Product identification was carried out through RP-UPLC-ESI-TOF-MS, as detailed earlier in the context of oligonucleotide synthesis.

5.4   UV melting temperature studies

The UV melting temperatures for equimolar (1.0 μM) mixtures of the cleaving agents **ON1x**, **ON1x-Hg**, **ON1y** and **ON1y-Hg₂** and target oligonucleotide were measured using a Perkin Elmer Lambda 35 UV–visible spectrometer that had a Peltier temperature controller unit. This spectrometer employed quartz cuvettes with a 10 mm optical path length and recorded the data at a wavelength of 260 nm. The temperature was gradually increased at a rate of 0.5 °C per minute, ranging from 10–90 °C. The measurements were conducted under pH 7.4 conditions in a 20 mM cacodylate buffer with an ionic strength of 0.10 M, which was adjusted using NaClO₄. An oligonucleotide concentration of 1.0 μM was used in all subsequent experiments. The melting temperatures (T_m) were identified as the points of inflection on the UV melting curves.

Acknowledgements

I am deeply grateful to Professor Tuomas Lönnberg, my Ph.D. supervisor, for his unparalleled expertise in the chemistry of oligonucleotides with organometallic modifications, as well as his extensive knowledge in organic/bioorganic chemistry. Throughout my Ph.D. journey, your supervision, encouragement, motivation, and invaluable guidance have been indispensable. Your patience and support, alongside your exceptional breadth of knowledge, have left a profound impact on me. Words cannot fully express my gratitude for your counseling and guidance during my time in Finland. The vast knowledge and skills you've shared have been crucial to my accomplishments. I extend special thanks to my co-supervisor, Dr. Mikko Ora, for his unwavering support and keen interest in my work. Your dedication to answering my questions and engaging in insightful discussions is greatly appreciated.

I want to thank the reviewers of this thesis, Professor James K. Bashkin and Professor David R. W. Hodgson, for finding the time in their busy schedule to read this thesis and make very valuable comments. I also want to thank Professor Roger Strömberg sincerely for agreeing to be my opponent.

I would like to extend my heartfelt gratitude to Professor Pasi Virta, Head of the Chemistry Department and leader of the Bioorganic Group, for your unwavering inspiration and invaluable guidance. Your cheerful demeanor and willingness to assist have made a significant impact on my journey, and I am deeply appreciative.

I express profound gratitude to the exceptional individuals with whom I have had the honor of working with within the Bioorganic Group. Their dedication and expertise have significantly enhanced my professional journey.

I would like to extend my heartfelt gratitude to Dr. Satu Mikkola, Dr. Heidi Korhonen, Dr. Petri Tähtinen, and Dr. Päivi Poijärvi-Virta. Their invaluable advice and enriching conversations on both chemistry and life in Turku have been

immensely appreciated. Additionally, I wish to express my deepest thanks to Kari Loikas, Kirsi Laaksonen, and Mauri Nauma for their unwavering support, which has enabled our team to operate seamlessly. I am also grateful to Dr. Alex Dickens, Dr. Jani Rahkila, Dr. Tuomas Karskela, and Dr. Denys Mavrynsky for their assistance with instrumentation, which has been crucial to our work in the chemistry department. Your contributions are indispensable and deeply valued.

Special acknowledgment is reserved for Dr. Madhuri A. Hande and Dr. Dattatraya Ukale, for their camaraderie and the enjoyable moments and whose insightful discussions and shared ideas have been instrumental in numerous successes and endeavors. Their contributions are not only notable but also deeply appreciated.

I would like to extend my heartfelt gratitude to Afari Mark, Dr. Asmo Aro-Heinilä, Aapo Aho, Dr. Vijay Gulumkar, Dr. Petja Rosenqvist, Dr. Tharun Kumar Kotammagari, Dr. Ville Tähtinen, Dr. Antti Äärelä, Toni Laine, Hanni Haapsaari, Verneri Saari, Heidi Kähkölä, Tommi Österlund, Akash James, and Dr. Sajal Maity for their invaluable friendship, the delightful moments shared, and the insightful discussions we've had. Your presence has not only been uplifting but also intellectually stimulating. I am truly grateful for the enriching conversations we've had, whether they were about chemistry (life) or the enjoyment of activities such as basketball, sauna sessions, bowling, swimming-*ish* 😊, ice-skating 😊, and football. Your camaraderie has greatly enhanced my overall experience, and for that, I am sincerely thankful.

I extend my heartfelt appreciation to the esteemed individuals comprising the Material and Intelligent Material Chemistry groups. I wish to express my gratitude to Sachin Kochrekar, Dr. Sami Vuori, Majid Al-waeel, Narhari Sapkota and Vinh Nguyen. Our collaborations have not only been intellectually stimulating but also immensely enjoyable. Each of you has played a pivotal role in nurturing a positive work atmosphere and cultivating a diverse international culture within our teams. I am particularly grateful to Adefunke Koyejo, Hanni, Mark and Asmo for our insightful discussions, which have not only been enriching but have also provided me with invaluable suggestions.
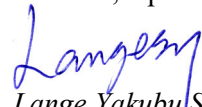
I am profoundly grateful to Esko Kukkasniemi, a cherished friend whose profound insights into Finnish culture and history have significantly enriched my understanding. Our conversations, spanning diverse topics, hold immense importance to me. Furthermore, I extend heartfelt thanks to Paul Abana, a childhood pal whose friendship has been invaluable in shaping my experiences and memories.

Completing this achievement has been made possible by the unwavering support of my family, to whom I owe immense gratitude. I wish to extend my deepest appreciation to my parents, Saleh and Dadale. Their unconditional love and unwavering support have served as guiding beacons throughout my academic

endeavors and life journey. Your encouragement, prayers, and heartfelt well-wishes have provided me with the strength to overcome challenges. Words cannot fully express the depth of my gratitude for the sacrifices you have made. Your unwavering belief in my capabilities has been a driving force, propelling me forward during difficult times. Your influence on both my academic thesis and personal life is immeasurable, and I am profoundly thankful for the values, wisdom, and love you have imparted to me. Thank you for being my rock, my inspiration, and my most ardent supporters. This achievement belongs to you as much as it does to me.

I also want to express my heartfelt gratitude to my beloved siblings – Iliya, Naomi, Yusuf, Ibrahim, and Ishaku – as well as to my wonderful nieces and nephews. Your constant love, support, trust, care, and encouragement have been invaluable companions on this journey. I am truly grateful for the profound connection we share. Additionally, reflecting on our shared upbringing, I realize there was never a dull moment; the notion of boredom seemed entirely foreign during those times.

Turku, April 2024

Lange Yakubu Saleh

List of References

[1]   Z. Zou, J. Wei, C. He, *Fundamental Research* **2023**, *3*, 760–762.

[2]   Y. Zhang, Q. Zhang, Y. Zhang, J. Han, *Int J Mol Sci* **2023**, *24*, 4939.

[3]   J. Micheel, A. Safrastyan, D. Wollny, *Noncoding RNA* **2021**, *7*, 70.

[4]   T. R. Mercer, M. E. Dinger, J. S. Mattick, *Nat Rev Genet* **2009**, *10*, 155–159.

[5]   P. C. Zamecnik, M. L. Stephenson, *PNAS* **1978**, *75*, 280–284.

[6]   S. Thakur, A. Sinhari, P. Jain, H. R. Jadhav, *Front Pharmacol* **2022**, *13*, DOI 10.3389/fphar.2022.1006304.

[7]   E. Uhlmann, A. Peyman, *Chem Rev* **1990**, *90*, 543–584.

[8]   C. Terada, S. Kawamoto, A. Yamayoshi, T. Yamamoto, *Pharmaceutics* **2022**, *14*, 2647.

[9]   M. Gagliardi, A. T. Ashizawa, *Biomedicines* **2021**, *9*, 433.

[10]   P. H. Hagedorn, B. R. Hansen, T. Koch, M. Lindow, *Nucleic Acids Res* **2017**, *45*, 2262–2282.

[11]   W. Shen, C. L. De Hoyos, M. T. Migawa, T. A. Vickers, H. Sun, A. Low, T. A. Bell, M. Rahdar, S. Mukhopadhyay, C. E. Hart, M. Bell, S. Riney, S. F. Murray, S. Greenlee, R. M. Crooke, X. Liang, P. P. Seth, S. T. Crooke, *Nat Biotechnol* **2019**, *37*, 640–650.

[12]   T. Yamaguchi, N. Horie, H. Aoyama, S. Kumagai, S. Obika, *Nucleic Acids Res* **2023**, *51*, 7749–7761.

[13]   L. Zhang, T. A. Vickers, H. Sun, X. Liang, S. T. Crooke, *Nucleic Acids Res* **2021**, *49*, 2721–2739.

[14]   E. RAYBURN, R. ZHANG, *Drug Discov Today* **2008**, *13*, 513–521.

[15]   Z. Dou, D. Zhao, X. Chen, C. Xu, X. Jin, X. Zhang, Y. Wang, X. Xie, Q. Li, C. Di, H. Zhang, *J. Exp. Clin. Cancer Res.* **2021**, *40*, 194.

[16]   R. L. Juliano, *Nucleic Acids Res* **2016**, *44*, 6518–6548.

[17]   T. R. Damase, R. Sukhovershin, C. Boada, F. Taraballi, R. I. Pettigrew, J. P. Cooke, *Front Bioeng Biotechnol* **2021**, *9*, DOI 10.3389/fbioe.2021.628137.

[18]   W.-Y. Tarn, Y. Cheng, S.-H. Ko, L.-M. Huang, *Pharmaceutics* **2021**, *13*, 2015.

[19]   S. T. Crooke, B. F. Baker, R. M. Crooke, X. Liang, *Nat Rev Drug Discov* **2021**, *20*, 427–453.

[20]   Ł. J. Kiełpiński, P. H. Hagedorn, M. Lindow, J. Vinther, *Nucleic Acids Res* **2017**, *45*, 12932–12944.

[21]   J. Kurreck, *Eur J Biochem* **2003**, *270*, 1628–1644.

[22]   M. A. Havens, M. L. Hastings, *Nucleic Acids Res* **2016**, *44*, 6549–6563.

[23]   O. V. Sergeeva, E. Y. Shcherbinina, N. Shomron, T. S. Zatsepin, *Nucleic Acid Ther* **2022**, *32*, 123–138.

[24]   M. Egli, M. Manoharan, *Nucleic Acids Res* **2023**, *51*, 2529–2573.

[25]   D. P. Bartel, *Cell* **2009**, *136*, 215–233.

[26]   A. Stark, J. Brennecke, N. Bushati, R. B. Russell, S. M. Cohen, *Cell* **2005**, *123*, 1133–1146.

[27]   A. Tahamtan, M. Teymoori-Rad, B. Nakstad, V. Salimi, *Front Immunol* **2018**, *9*, DOI 10.3389/fimmu.2018.01377.

[28]   C. Li, Z. Zhou, C. Ren, Y. Deng, F. Peng, Q. Wang, H. Zhang, Y. Jiang, *Front Pharmacol* **2022**, *13*, DOI 10.3389/fphar.2022.1007723.

[29]   I. Kimsey, H. M. Al-Hashimi, *Curr Opin Struct Biol* **2014**, *24*, 72–80.

[30] S. Qi, N. Duan, I. M. Khan, X. Dong, Y. Zhang, S. Wu, Z. Wang, *Biotechnol Adv* **2022**, *55*, 107902.

[31] L. Zhu, J. Yang, Y. Ma, X. Zhu, C. Zhang, *J Am Chem Soc* **2022**, *144*, 1493–1497.

[32] A. D. Keefe, S. Pai, A. Ellington, *Nat Rev Drug Discov* **2010**, *9*, 537–550.

[33] K. D. Kovacevic, J. C. Gilbert, B. Jilma, *Adv Drug Deliv Rev* **2018**, *134*, 36–50.

[34] A. Bortolozzi, S. Manashirov, A. Chen, F. Artigas, *Pharmacol Ther* **2021**, *227*, 107873.

[35] N. H. Williams, P. Wyman, *ChemComm* **2001**, 1268–1269.

[36] M. Komiyama, *Chem Lett* **2016**, *45*, 1347–1355.

[37] S. Mikkola, T. Lönnberg, H. Lönnberg, *Beilstein J. Org. Chem.* **2018**, *14*, 803–837.

[38] H. Lönnberg, *Org Biomol Chem* **2011**, *9*, 1687.

[39] F. H. Westheimer, *Acc Chem Res* **1968**, *1*, 70–78.

[40] R. Wolfenden, C. Ridgway, G. Young, *J Am Chem Soc* **1998**, *120*, 833–834.

[41] K. S. Gates, *Chem Res Toxicol* **2009**, *22*, 1747–1760.

[42] G. K. Schroeder, C. Lad, P. Wyman, N. H. Williams, R. Wolfenden, *PNAS* **2006**, *103*, 4052–4055.

[43] P. Jarvinen, M. Oivanen, H. Lonnberg, *J Org Chem* **1991**, *56*, 5396–5401.

[44] R. Wolfenden, M. J. Snider, *Acc Chem Res* **2001**, *34*, 938–945.

[45] Y. Li, R. R. Breaker, *J Am Chem Soc* **1999**, *121*, 5364–5372.

[46] M. Oivanen, S. N. Mikhailov, N. Sh. Padyukova, H. Lonnberg, *J Org Chem* **1993**, *58*, 1617–1619.

[47] M. Kosonen, E. Yousefi-Salakdeh, R. Strömberg, H. Lönnberg, *J. Chem. Soc., Perkin Trans. 2* **1998**, 1589–1596.

[48] R. Breslow, S. D. Dong, Y. Webb, R. Xu, *J Am Chem Soc* **1996**, *118*, 6588–6600.

[49] Ronald. Breslow, Marc. Labelle, *J Am Chem Soc* **1986**, *108*, 2655–2659.

[50] E. Anslyn, R. Breslow, *J Am Chem Soc* **1989**, *111*, 4473–4482.

[51] M. Forconi, D. Herschlag, in *Methods Enzymol*, **2009**, pp. 91–106.

[52] A. Chatterjee, K. Zhang, Y. Rao, N. Sharma, D. E. Giammar, K. M. Parker, *Environ Sci Technol* **2022**, *56*, 3564–3574.

[53] X. Liu, Y. Chen, C. A. Fierke, *J Am Chem Soc* **2017**, *139*, 17457–17463.

[54] Q. Hu, V. M. Jayasinghe-Arachchige, J. Zuchniarz, R. Prabhakar, *Front Chem* **2019**, *7*, DOI 10.3389/fchem.2019.00195.

[55] T. A. Steitz, J. A. Steitz, *PNAS* **1993**, *90*, 6498–6502.

[56] M. Dano, M. Elmeranta, D. R. W. Hodgson, J. Jaakkola, H. Korhonen, S. Mikkola, *J. Biol. Inorg. Chem.* **2015**, *20*, 1299–1306.

[57] H. Korhonen, T. Koivusalo, S. Toivola, S. Mikkola, *Org Biomol Chem* **2013**, *11*, 8324.

[58] R. Breslow, D. L. Huang, *PNAS* **1991**, *88*, 4080–4083.

[59] K. Matsumura, M. Komiyama, *J Biochem* **1997**, *122*, 387–394.

[60] K. Le Vay, E. Salibi, E. Y. Song, H. Mutschler, *Chem Asian J* **2020**, *15*, 214–230.

[61] W. R. Farkas, *Biochim Biophys Acta Nucleic Acids Protein Synth* **1968**, *155*, 401–409.

[62] W. Yang, *Q Rev Biophys* **2011**, *44*, 1–93.

[63] Y. Staroseletz, S. Gaponova, O. Patutina, E. Bichenkova, B. Amirloo, T. Heyman, D. Chiglintseva, M. Zenkova, *Molecules* **2021**, *26*, 1732.

[64] D. M. Perrin, in *Polymer Science: A Comprehensive Reference*, Elsevier, **2012**, pp. 3–33.

[65] A. Serganov, S. Keiper, L. Malinina, V. Tereshko, E. Skripkin, C. Höbartner, A. Polonskaia, A. T. Phan, R. Wombacher, R. Micura, Z. Dauter, A. Jäschke, D. J. Patel, *Nat Struct Mol Biol* **2005**, *12*, 218–224.

[66] K. Jijakli, B. Khraiwesh, W. Fu, L. Luo, A. Alzahmi, J. Koussa, A. Chaiboonchoe, S. Kirmizialtin, L. Yen, K. Salehi-Ashtiani, *Methods* **2016**, *106*, 3–13.

[67] H. Peng, B. Latifi, S. Müller, A. Lupták, I. A. Chen, *RSC Chem Biol* **2021**, *2*, 1370–1383.

[68] H. Ge, M. A. Marchisio, *Life* **2021**, *11*, 248.

[69] R. Micura, C. Höbartner, *Chem Soc Rev* **2020**, *49*, 7331–7353.

[70] J. Deng, Y. Shi, X. Peng, Y. He, X. Chen, M. Li, X. Lin, W. Liao, Y. Huang, T. Jiang, D. M. J. Lilley, Z. Miao, L. Huang, *Nucleic Acids Res* **2023**, *51*, D262–D268.

[71] T. Lönnberg, *Chem. - Eur. J.* **2011**, *17*, 7140–7153.

[72] D. Alonso, A. Mondragón, *Biochem Soc Trans* **2021**, *49*, 1529–1535.

[73] T. Lönnberg, H. Lönnberg, *Curr Opin Chem Biol* **2005**, *9*, 665–673.

[74] A. Kuzuya, M. Komiyama, *Curr Org Chem* **2007**, *11*, 1450–1459.

[75] A. Ghidini, M. Murtola, R. Strömberg, in *DNA in Supramolecular Chemistry and Nanotechnology*, Wiley, **2014**, pp. 158–171.

[76] T. Niittymäki, H. Lönnberg, *Org Biomol Chem* **2006**, *4*, 15–25.

[77] D. Hüsken, A. Deichert, J. Hall, R. Häner, *Nucleosides Nucleotides* **1999**, *18*, 1507–1511.

[78] K. Matsumura, M. Endo, M. Komiyama, *J. Chem. Soc., Chem. Commun.* **1994**, 2019–2020.

[79] T. Niittymäki, E. Burakova, E. Laitinen, A. Leisvuori, P. Virta, H. Lönnberg, *Helv Chim Acta* **2013**, *96*, 31–43.

[80] B. N. Trawick, T. A. Osiek, J. K. Bashkin, *Bioconjug Chem* **2001**, *12*, 900–905.

[81] J. Hall, D. Hüsken, U. Pieles, H. E. Moser, R. Häner, *Chem Biol* **1994**, *1*, 185–190.

[82] Y. Staroseletz, A. Williams, K. K. Burusco, I. Alibay, V. V. Vlassov, M. A. Zenkova, E. V. Bichenkova, *Biomaterials* **2017**, *112*, 44–61.

[83] O. Patutina, D. Chiglintseva, E. Bichenkova, S. Gaponova, N. Mironova, V. Vlassov, M. Zenkova, *Molecules* **2020**, *25*, 2459.

[84] Y. Staroseletz, B. Amirloo, A. Williams, A. Lomzov, K. K. Burusco, D. J. Clarke, T. Brown, M. A. Zenkova, E. V. Bichenkova, *Nucleic Acids Res* **2020**, *48*, 10662–10679.

[85] T. Sunami, J. Kondo, I. Hirao, K. Watanabe, K. Miura, A. Takénaka, *Acta Crystallogr D Biol Crystallogr* **2004**, *60*, 90–96.

[86] O. A. Patutina, S. K. Miroshnichenko, N. L. Mironova, A. V. Sen'kova, E. V. Bichenkova, D. J. Clarke, V. V. Vlassov, M. A. Zenkova, *Front Pharmacol* **2019**, *10*, DOI 10.3389/fphar.2019.00879.

[87] O. A. Patutina, M. A. Bazhenov, S. K. Miroshnichenko, N. L. Mironova, D. V. Pyshnyi, V. V. Vlassov, M. A. Zenkova, *Sci Rep* **2018**, *8*, 14990.

[88] J. Hall, *Nucleic Acids Res* **1996**, *24*, 3522–3526.

[89] T. Niittymäki, P. Virta, K. Ketomäki, H. Lönnberg, *Bioconjug Chem* **2007**, *18*, 1583–1592.

[90] N. G. Beloglazova, M. M. Fabani, N. N. Polushin, V. V. Sil'nikov, V. V. Vlassov, E. V. Bichenkova, M. A. Zenkova, *J Nucleic Acids* **2011**, *2011*, 1–17.

[91] F. Danneberg, A. Ghidini, P. Dogandzhiyski, E. Kalden, R. Strömberg, M. W. Göbel, *Beilstein J. Org. Chem.* **2015**, *11*, 493–498.

[92] P. Dogandzhiyski, A. Ghidini, F. Danneberg, R. Strömberg, M. W. Göbel, *Bioconjug Chem* **2015**, *26*, 2514–2519.

[93] F. Zellmann, L. Thomas, U. Scheffer, R. Hartmann, M. Göbel, *Molecules* **2019**, *24*, 807.

[94] O. A. Patutina, E. V. Bichenkova, S. K. Miroshnichenko, N. L. Mironova, L. T. Trivoluzzi, K. K. Burusco, R. A. Bryce, V. V. Vlassov, M. A. Zenkova, *Biomaterials* **2017**, *122*, 163–178.

[95] A. Williams, Y. Staroseletz, M. A. Zenkova, L. Jeannin, H. Aojula, E. V. Bichenkova, *Bioconjug Chem* **2015**, *26*, 1129–1143.

[96] O. Luige, M. Murtola, A. Ghidini, R. Strömberg, *Molecules* **2019**, *24*, 672.

[97] M. Murtola, M. Wenska, R. Strömberg, *J Am Chem Soc* **2010**, *132*, 8984–8990.

[98] M. Murtola, A. Ghidini, P. Virta, R. Strömberg, *Molecules* **2017**, *22*, 1856.

[99] H. Inoue, T. Furukawa, M. Shimizu, T. Tamura, M. Matsui, E. Ohtsuka, *ChemComm* **1999**, 45–46.

[100] W. C. Putnam, J. K. Bashkin, *J Inorg Biochem* **2022**, *232*, 111831.

[101] J. Hauptmann, V. Hehne, M. Balzer, L. Bethge, M. Wikstrom Lindholm, *Mol Ther Nucleic Acids* **2022**, *27*, 1116–1126.

[102] A. D. Saleh, P. S. Miller, *Nucleos. Nucleot. Nucl.* **2011**, *30*, 235–255.

[103] M. A. Reynolds, T. A. Beck, P. B. Say, D. A. Schwartz, B. P. Dwyer, W. J. Daily, M. M. Vaghefi, M. D. Metzler, R. E. Klem, L. J. Arnold, *Nucleic Acids Res* **1996**, *24*, 760–765.

[104] D. Ossipov, R. Strömberg, *Nucleos. Nucleot. Nucl.* **2005**, *24*, 901–905.

[105] O. Luige, P. P. Bose, R. Stulz, P. Steunenberg, O. Brun, S. Andersson, M. Murtola, R. Strömberg, *ChemComm* **2021**, *57*, 10911–10914.

[106] N. Iwamoto, D. C. D. Butler, N. Svrzikapa, S. Mohapatra, I. Zlatev, D. W. Y. Sah, Meena, S. M. Standley, G. Lu, L. H. Apponi, M. Frank-Kamenetsky, J. J. Zhang, C. Vargeese, G. L. Verdine, *Nat Biotechnol* **2017**, *35*, 845–851.

[107] N. N. Polushin, *Nucleic Acids Res* **2000**, *28*, 3125–3133.

[108] N. G. Beloglazova, *Nucleic Acids Res* **2004**, *32*, 3887–3897.

[109] M. Gaglione, G. Milano, A. Chambery, L. Moggio, A. Romanelli, A. Messere, *Mol Biosyst* **2011**, *7*, 2490.

[110] D. Magda, M. Wright, S. Crofts, A. Lin, J. L. Sessler, *J Am Chem Soc* **1997**, *119*, 6947–6948.

[111] M. Murtola, R. Strömberg, *Org Biomol Chem* **2008**, *6*, 3837.

[112] J. Li, M. Mohammed-Elsabagh, F. Paczkowski, Y. Li, *ChemBioChem* **2020**, *21*, 1547–1566.

[113] M. Cepeda-Plaza, E. L. Null, Y. Lu, *Nucleic Acids Res* **2013**, *41*, 9361–9370.

[114] M. Hollenstein, *Chimia (Aarau)* **2011**, *65*, 770.

[115] G. Paolella, B. S. Sproat, A. I. Lamond, *EMBO J* **1992**, *11*, 1913–1919.

[116] H. Almer, J. Stawinski, R. Stroemberg, M. Thelin, *J Org Chem* **1992**, *57*, 6163–6169.

[117] Y. Xu, Y. Suzuki, T. Lönnberg, M. Komiyama, *J Am Chem Soc* **2009**, *131*, 2871–2874.

[118] T. Lönnberg, Y. Suzuki, M. Komiyama, *Org Biomol Chem* **2008**, *6*, 3580.

[119] T. A. Henry, T. M. Sharp, *J. Chem. Soc., Trans.* **1922**, *121*, 1055–1060.

[120] S. K. Maity, T. A. Lönnberg, *ACS Omega* **2019**, *4*, 18803–18808.

[121] J.-L. Mergny, L. Lacroix, *Oligonucleotides* **2003**, *13*, 515–537.

[122] R. B. Simpson, *J Am Chem Soc* **1964**, *86*, 2059–2065.

[123] A. D. Collins, P. De Meester, D. M. L. Goodgame, A. C. Skapski, *Biochim Biophys Acta Nucleic Acids Protein Synth* **1975**, *402*, 1–6.

[124] J.-L. Leroy, M. Guéron, *Biochimie* **1982**, *64*, 297–299.

[125] J. Louis. Leroy, Maurice. Gueron, *J Am Chem Soc* **1986**, *108*, 5753–5759.

[126] M. Ora, H. Linjalahti, H. Lönnberg, *J Am Chem Soc* **2005**, *127*, DOI https://doi.org/10.1021/ja045060+.

[127] J. P. Charland, Phan Viet Minh Tan, M. St-Jacques, A. L. Beauchamp, *J Am Chem Soc* **1985**, *107*, 8202–8211.

[128] S. E. Taylor, E. Buncel, A. R. Norris, *J Inorg Biochem* **1981**, *15*, 131–141.

[129] M. Oivanen, M. Ora, H. Almer, R. Stromberg, H. Lonnberg, *J Org Chem* **1995**, *60*, 5620–5627.

[130] P.-J. J. Huang, F. Wang, J. Liu, *Anal Chem* **2015**, *87*, 6890–6895.

[131] H. Lönnberg, H. Svanholt, A. Holm, *Acta Chem Scand* **1980**, *34a*, 703–708.

**TURUN
YLIOPISTO**
UNIVERSITY
OF TURKU